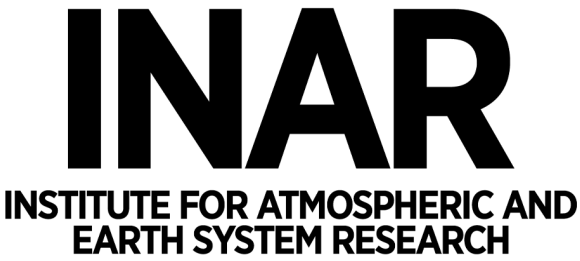

Masters Thesis
Geophysics of the Hydrosphere

Characterization of a small high-Arctic glacier system via historical observations and numerical modelling

Tomi Walter Vainio

March 18, 2022

Supervisor(s): Prof. Andy Hodson, Docent Thomas Zwinger

Examiner(s): Prof. Andy Hodson
Prof. Petteri Uotila

UNIVERSITY OF HELSINKI
Department of Physics

PL 64 (Gustaf Hällströmin katu 2a)
00014 Helsingin yliopisto

HELSINGIN YLIOPISTO — HELSINGFORS UNIVERSITET — UNIVERSITY OF HELSINKI

Tiedekunta — Fakultet — Faculty	Laitos — Institution — Department
Faculty of Science	Department of Physics

Tekijä — Författare — Author
Tomi Walter Vainio

Työn nimi — Arbetets titel — Title
Characterization of a small high-Arctic glacier system via historical observations and numerical modelling

Oppiaine — Läroämne — Subject
Geophysics of the Hydrosphere

Työn laji — Arbetets art — Level	Aika — Datum — Month and year	Sivumäärä — Sidoantal — Number of pages
Masters Thesis	March 18, 2022	81

Tiivistelmä — Referat — Abstract

Small arctic glaciers have in general been consistently neglected with respect to the collection of long time-series observations. Available data is often a product of multiple independent and separate studies, thus gaps in the data sets are common. Numerical modelling provides one solution to alleviate existing gaps in knowledge, while historical observations can be used to assess model accuracy.

The Foxfonna ice cap and associated glacier were investigated with the aid of the numerical modelling software, Elmer/Ice. The goal was to reproduce core glaciological characteristics of the entire glacier system from a 3D simulation based on multiple digital elevation models (DEMs) between the years 1961-2021. Simulations of the following parameters were produced and tuned against existing data where possible: surface mass balance (1961-2020), isochrone distribution (1961 & 2020), ice flow velocity (1961 & 2020) and ice temperature (1972). The surface mass balance simulations proved to match available in situ measurements (sim. avg. -0.52 m w.eq., obs. -0.51 m w.eq.) for 2009-2020 (Table 5.3), while other time periods either lacked data or were affected by gaps in the series. Isochrone simulations proved a poor match for reality. Ice within the core of Foxfonna was 2000-3000 years in age, which is up to twice the age of ice-marginal mosses revealed by glacier retreat. However, the simulation relies heavily on the assumption of a steady state, which does not apply to the rapidly melting Foxfonna. The simulated flow of the glacier ice underestimated velocities slightly on the lower glacier, but matched observations on the ice cap rather well. Both the model and observations provide velocities up to 0.3 m/a for the ice cap, except for one outlier. The simulations of the valley glacier matched poorly to the observations. However, the velocity measurements were patchy and provided only a snapshot of the glacier, and so any observational errors were not averaged out by repeat measurements.

The methods proved capable of providing additional information on the glaciological characteristics of a small glacier system, such as Foxfonna. Issues primarily arose from the steady state assumption and the difficulty of producing simulations for a dynamically varying glacier system.

Avainsanat — Nyckelord — Keywords
Foxfonna, Svalbard, Spitsbergen, Elmer/Ice, surface mass balance, finite-element modelling

Säilytyspaikka — Förvaringsställe — Where deposited

Muita tietoja — övriga uppgifter — Additional information

Contents

List of Figures

List of Tables

Acknowledgements

To start off with, I would like to thank my supervisors, Professor Andy Hodson, and Docent Thomas Zwinger. Andy, your ideas and support are what has allowed me to work within the environment I most enjoy. I am especially grateful for the many days in the field I have been able to partake as a part of the research group, and that you always made time for a chat when needed. Thomas, thank you sharing your expertise with Elmer/Ice - this thesis would not have been possible without your guidance! Your calmness and kindness in teaching helped me learn more than I expected. My gratitude also goes out to Professor Petteri Uotila, whose calm encouragement and support helped me in finishing my thesis on Svalbard. I feel that if any one of you three was missing, I would not have managed a similar project.

I owe a debt to Wilson Wai Yin Cheung. As a part of his own Msc thesis, he created a basal DEM of the glacier system, which was crucial for my own work. To Max Nuessle, who helped me with my Linux troubles, and to my cheery, uplifting office mates in room 309, Marjolein, Lotte, Nil, and Regine.

My gratitude goes out to the Department of Physics at the University of Helsinki for my education, and to the local student organisations - especially Resonanssi ry - for giving me a place like home during my studies in Helsinki. I am also very grateful for the funding I've received from Maa- ja Vesitekniikan Tuki ry (MVTT) and the Erasmus programme, as well as the support provided by the University Centre in Svalbard, without which this project would have been difficult to complete.

My love and gratitude goes out to my parents, Lisa and Erkko, whom I care for dearly, and who have supported me throughout my life. Without them I would likely not be finishing my degree in the Arctic. I also love my brother, Joni, although it has been better for everyone that his "scientific advice" never made it into my thesis.

1. Introduction

1.1 Glaciers within the cryosphere

Glaciers are large masses of ice flowing slowly under their own weight; the movement of glacier ice resembles that of an extremely viscous fluid. The flow of glacier ice erodes and shapes the landscape underneath it; most valleys in the archipelago of Svalbard have been formed during the many glacial periods of the past. In general, glaciers are located in the high-altitude or polar regions of the world as they require perennially or near-perennially cold climates, with at least some precipitation in order to sustain a persistent snow cover on parts of the glacier surface (see Figure 1.1). As the precipitation from multiple years accumulates the snow at the bottom becomes denser as it is compressed. Eventually this snow is dense enough to be considered firn and therefore is on its way to becoming glacier ice [Benn D., 2010], [Cuffey and Paterson, 2010].

As such glaciers themselves are a reflection of the local climate; though sometimes that of a past one. Many have grown during the favorable conditions of previous millennia, which may no longer be present, in part due to the recent effects of anthropogenic climate change, which is known to affect the extent of glaciation [Vaughan et al., 2013]. Glaciation on Svalbard is still prevalent due to the nearly year-round subzero temperatures afforded to the archipelago by its extremely northern location (see Section 1.4.1, "Climate"). Some 40% of total glaciation on Svalbard consists of smaller valley, or alpine glaciers [Blaszczyk et al., 2009]. In total glaciers cover some 56% of the archipelago [Nuth et al., 2013], although this extent is down from 60% in 1993 [Hagen et al., 1993].

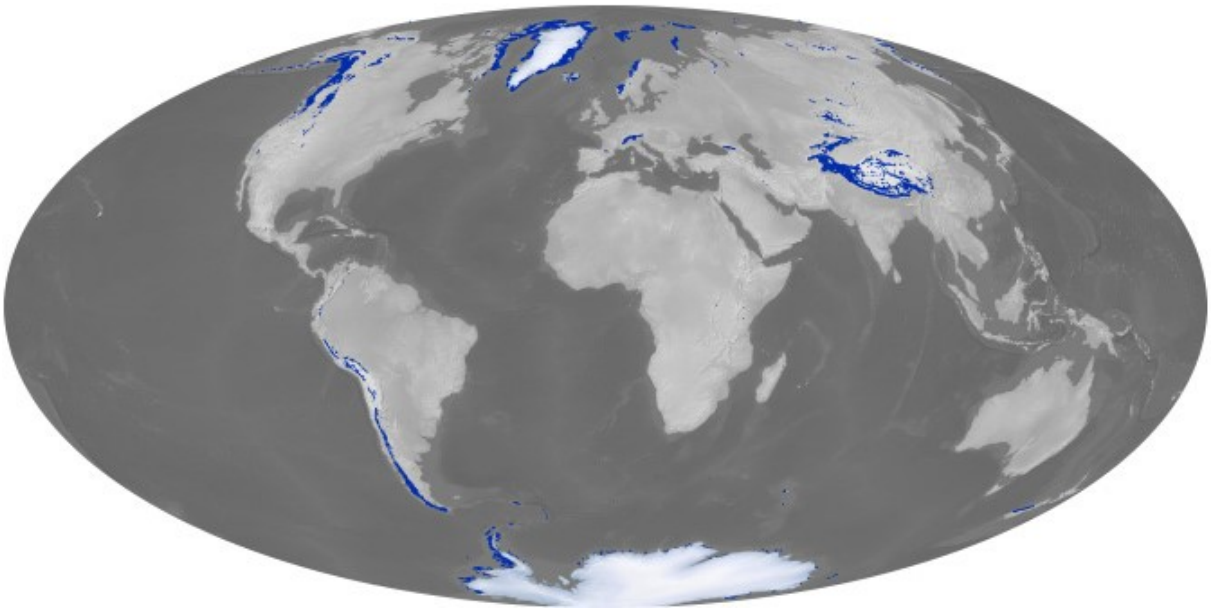

Figure 1.1: Contemporary glaciation takes place in high-latitude or altitude regions where the local climate allows for colder annual temperatures. The figure showcases the 2014 extent (in blue) of all the glaciers, ice sheets, and ice caps on planet Earth [Pfeffer et al., 2014].

Receding glaciers are in part a sign of climate change [Vaughan et al., 2013]. However the rate at which glaciers react to a changing climate varies. While larger ice sheets may react on a centurial scale to the effects of any changes within the climate system, smaller - especially shorter - glaciers can react much faster [Brugger, 2007], [Salinger et al., 2008], with many smaller glaciers retreating since the late 1900's. This reduction is also partly due to the albedo effect of anthropogenic particulates [Flanner et al., 2007], [Doherty et al., 2010], [Painter et al., 2013]. Some of these can be accredited to atmospheric black carbon deposition from early 1850's industry, instead of direct, observable climate effects [Painter et al., 2013]. The presence of pollutants - natural or other - is often visible on the glacier surface, as each successive year of accumulation forms its own layer, akin to growth-rings on a tree. Each ring reveals the presence of an isochrone, a layer of ice with the same age due to being deposited during the same accumulation period. These layers of ice can provide valuable information on past atmospheric conditions [Legrand et al., 1988], [Isakson et al., 2005], and could yield information from the particulates deposited onto the surface, both natural and anthropogenic [Koziol, 2014].

The study of glaciers is often undertaken due to varying motivations and goals. For many they provide an important source of fresh water, while others are concerned by their contribution to sea level change. Both are interested in the same goal, but for different reasons. Both can benefit from the same information (e.g. the annual mass budget). This information has historically been collected with in situ measurements, such as using ablation stakes in the ice to monitor surface changes or to track the movement of ice. Despite their valuable data contribution, stake measurements are point measurements by definition, thus leaving gaps in our understanding. Contemporary methods, such as the use of remote sensing, numerical modelling, and digital elevation models, have provided motivated scientists with the ability to fill in these gaps of knowledge - provided that the input data is of sound quality.

Figure 1.2: The Foxfonna ice cap as seen from above. The glacier of Fleinisen and the valley of Foxdalen can be seen in the background. Image is oriented towards the east and provided courtesy of Wilson Wai Yin Cheung.

1.2 The complementary roles of field observations and glacier modelling

Observation of the natural world is a foundation of nearly all fields of science to date, and the core principles of natural forces and/or phenomena are for the most part well understood within the contemporary world. However, while a well executed field campaign can provide concrete data on specific parameters, there are often inherent shortcomings in this approach. Taking glaciers as an example, it is often cost- or time-prohibitive, dangerous, or even impossible to cover the entire area of interest. And at times it can be impossible to reach a planned goal with only in situ data of the present moment. Such shortcomings can at times be fixed by some manner of interpolation based on observations. But simple interpolation may be insufficient due to the inherent complexity of the system or some poorly constrained parameters. A solution to this is numerical models, such as a simple linear or first-order model of a glacier system, such as a Shallow Ice Approximation (SIA), or even a fully realized numerical model, e.g. a full-Stokes model [Fowler et al., 2019].

Numerical models are extremely useful in providing a complete understanding of the natural system, especially one from the past. Historical records on glacier dynamics or mass balance are sparse, but combining numerical modelling with other techniques - such as orthophotogrammetry - it is possible produce simulated data sets on glacier dynamics and mass balance from before the existence of consistent instrumental records [Välisuo et al., 2017], [Peyaud et al., 2020]. However, if consistent data sets exist of a glacier, it is also possible to simulate an educated forecast of future glacier ice volume and dynamics [Seddik et al., 2012], [Peyaud et al., 2020]. Other applications include estimating glacier-hazards [Gagliardini et al., 2011], [Gilbert et al., 2018] providing solutions to the historical or future dynamics of small valley glaciers [Zwinger et al., 2009], [Adhikari et al., 2012], debris tracking within glacier ice [Jouvet et al., 2020], and estimating the variability of glacier melt [Edwards et al., 2021], [Malles et al., 2021] and ice-sheet melt [Edwards et al., 2014] on sea level rise.

The computational demand of a model increases with added complexity and detail. Some models, such as those related to glaciers systems, can require only few input parameters besides geometry and general topography. This allows for estimates across the entire glacier to be produced only after a day or two of fieldwork. Compared to trying to monitor glacier movement using an ablation stake network - which provides only point data and can miss the fastest flow if poorly located - this is a very positive trait of simulating a system. Furthermore, modelling is a valid method of providing insight into the accuracy of historical measurements through re-analysis, such as in [Andreassen et al., 2016], [O'Neel et al., 2019].

However, are simulated results trustworthy? The worse the quality of the input parameters are, the worse the output will be - known as "Garbage In, Garbage Out". Simulations are a great tool in solving or approximating for unknowns - especially spatial ones - but require real-world observations which allow the user to adjust input parameters so the model matches reality, such as in [Zwinger et al., 2009], [Zwinger et al., 2014], [Compagno et al., 2019]. It is prudent to keep in mind that poorly executed real-world observations provide poor values to verify against; it is thus ideal to have repeat measurements, but if lacking long-term observations then a healthy skepticism is prudent. It is obvious that neither approach - observation and simulation - is exclusive. Rather they complement each other by providing information beyond the ability of any individual person or field campaign, which can then be constrained as well as verified by repeat measurements done in the field.

1.3 Background and objectives

The initial motivation for this study was the tracking of stored anthropogenic pollution, in part to reconstruct past impact of human activities in a post-industrial society. As with other glaciers, anthropogenic pollutants have been deposited onto the surface of Foxfonna since the advent of the industrial revolution in the 1800's [Schwikowski and Eichler, 2010], [Fowler et al., 2019]. In the past these pollutants have been retained within the annual snow cover and subsequently within the glacier - annual layers of ice which are known as isochrones. Now as the glacier is consistently losing mass, many of these stored pollutants are being released downstream from the melting ice. It is of interest to know more, e.g. where from and how fast these pollutants will be released. This can be achieved by numerical modelling of the glacier and the age of its ice.

Furthermore, the Foxfonna glacier system has been poorly covered from a glaciological perspective, with only [Liestol, 1974], [Christiansen et al., 2005], [Rutter et al., 2011], [Koziol, 2014], and [Hodson et al., 2020] providing limited and intermittent glaciological data on the site, thus resulting in an incomplete picture of the study site. In order to better provide for the primary focus of the study it was useful to compile known data as a summary of the glaciological characteristics of the Foxfonna glacier system from which to build upon by numerical modelling.

Aims and Objectives

This thesis aims to evaluate the feasibility of using the available data and understanding of the Foxfonna glacier system in order to model it accurately with Elmer/Ice, a numerical modelling software. To reach this aim, the following objectives are set:

- Synthesize data describing the dynamic and climatic characteristics of Foxfonna
- Simulate the flow of ice, age of ice, and surface mass balance of the Foxfonna glacier system using Elmer/Ice
- Compare the simulated values to empirical data in order to assess the accuracy of simulations

1.4 Study Area

The study area consists of the Foxfonna ice cap, as well as an alpine-type valley glacier, the Foxfonna glacier, located within [78°07'14N–78°09'08N; 16°04'00E–16°13'00E] (see Figure 1.3). Both are situated within an elevation range of 350-809 m.a.s. on or next to the plateau mountain of Breinosa, with the Foxfonna glacier forming on the mountains northern slope. Further details on both the ice cap and valley glacier are provided next.

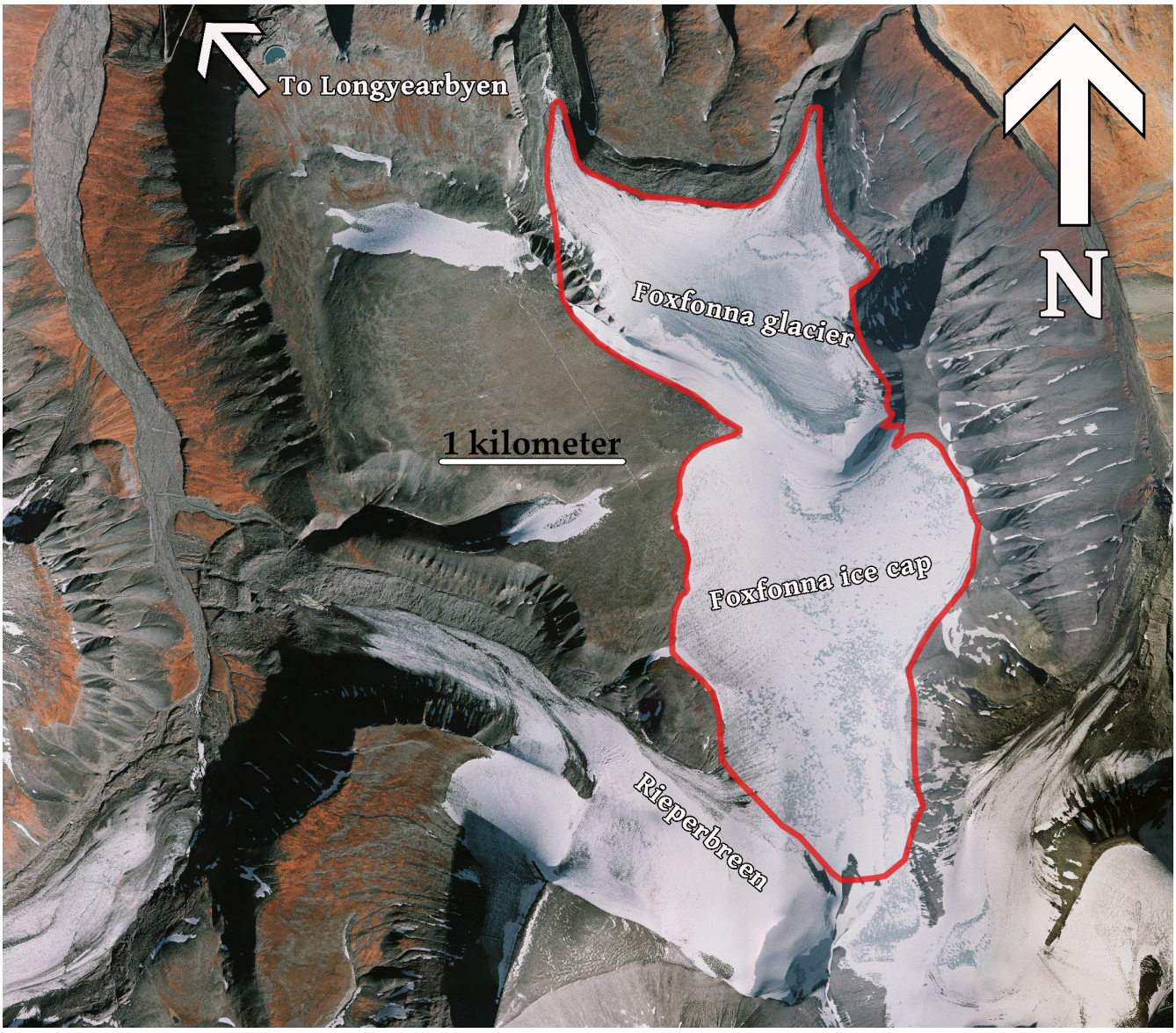

Figure 1.3: Outline (in red) of the study area (circa 1961) - the Foxfonna glacier system. The approximate direction of Longyearbyen and geographic north are included, as well as the location of the Rieperbreen glacier south of the ice cap. Imagery courtesy of the Norwegian Polar Institute (NPI).

Foxfonna ice cap

The Foxfonna ice cap is a thin, button-shaped mass of ice with a present day maximum thickness of 70 meters (yr. 2021). It sits on top of Breinosa - a plateau mountain - flowing outwards in a radial pattern. To the north it connects to the lower Foxfonna glacier via an ice fall, while to the south it follows a gentler slope into Rieperbreen. To its west and east it faces no obstructions.

The Foxfonna ice cap is a textbook example of a cold-based glacier, as surface ice velocities range from 0.15 to 0.3 m/a [Koziol, 2014] and there is no evidence to support a warm glacier bed. The same study found one point of the glacier moving at almost 1 m/a, the value is an outlier and a possible measurement error, as the observed flow direction is perpendicular to the elevation gradient.

The cold-based nature of the glacier is largely due to local climate and glacier geometry; Foxfonna ice cap is not thick enough to sufficiently raise the pressure melting point at the glacier bed, nor thick enough to insulate the bed in order to counter the near-perennially cold atmospheric temperatures which the Arctic environment offers. In addition, the underlying ground is permafrost, supporting the argument for colder temperatures at the glacier bed. This thermal regime can also be inferred from field campaigns, such as two ground-penetrating radar studies, one in 2021 [Cheung, 2021], another in 2012-2014 [Koziol, 2014] showing a clear reflection from the glacier bed; strong evidence of a dry bed. As well as from a sample of undisturbed moss discovered at the glacier margin, estimated at around 1500 years old [Roche, 2021]; a sliding (i.e. "warm"-, or "wet"-based) glacier would not have preserved the moss.

Between 1961 and 2021 the ice cap has retained its shape, but shrunk in area and thickness. Loss of area has occurred primarily on its western, south-western, and south-eastern sides [Koziol, 2014], while conversely to normal accumulation patterns there is considerable mass loss at the highest point. This is likely due to the peaks exposure to wind and solar radiation which could

historically have been counteracted by lower ablation in the colder summers allowing for snow to be retained. Maximum ice thickness has decreased from around 89 m (1961 yr.) to 70 m (2021 yr.). Mass balance observations conducted since 2007 show a consistent trend of thinning, with an annual mean mass loss of around 0.4 m.w.e (see Table 3.3, Figure 3.3) which is a typical, but slightly higher value for a Svalbard glacier [Rutter et al., 2011], [Hodson et al., 2020]. Higher rates of thinning have been observed on Svalbard e.g. with a mass loss of around 0.6 m.w.e on Midtre Lovénbreen [Kohler et al., 2003], [Kohler et al., 2007], [Välisuo et al., 2017]. However Foxfonna ice cap resides at high elevation from ~730 to 809 m.a.s.l, while Midtre Lovénbreen ranges from 50 to 650 m.a.s.l. As such the latter experiences warmer air temperatures and subsequently more melting.

Foxfonna glacier

Foxfonna glacier is an alpine-type valley glacier flowing northwards into two distinct valleys, with the two tongued flow forming a shape akin to a fox's ears. To the south it forms a cauldron which is connected to the Foxfonna ice cap via a steep slope. The ice is at its thickest inside the cauldron - some 115 meters. To the east-west it is bordered by the Breinosa massif.

Similar to the ice cap above, the contemporary Foxfonna glacier is assumed to be entirely cold-based due to its geometry in relation to the local climate; it is a thin glacier in a cold environment (See Figures 1.4). This is supported by ice temperature measurements showing -4.4°C at around 35 meters depth, and basal temperatures ranging from of -3.3°C at the center of the glacier, to -6.7°C near the glacier tongue [Liestol, 1974]. Furthermore, temperature observations of the underlying bedrock have shown values well below 0°C [Christiansen et al., 2005]. However recent measurements revealed temperate ice; up to 20 meters above the bed [Cheung, 2021]. It seems unlikely that a fifth of the total ice thickness is composed of temperate ice and the topic requires further investigation. It is possible that ice near the glacier bed is temperate and similar findings were reported by [Koziol, 2014].

Surface velocities measured in 2012-2014 show that the glacier is moving very slowly, only some 0.3 to 3 m/a [Koziol, 2014]. These velocities are consistent with the assumed cold-based nature of the glacier. Unfortunately the current surface velocity observations cover only the western flow path and are unique.

The Foxfonna valley glacier has been experiencing severe mass loss in the recent decades; its maximum thickness has reduced from 130 m (1961) to 115 m (2021). Between 1990-2012 it has lost on average 0.74 ± 0.10 m.w.e annually, notably at the glacier tongue (1.5 m.w.e between 1990-2009) [Koziol, 2014]. Due to the warm summers and moderate altitude ranges it is common for melting to occur over the entire glacier surface.

1.4.1 Climate

Classified as an Arctic tundra, the Svalbard archipelago experiences below freezing temperatures for two-thirds of the year and very little precipitation in general (see Figure 1.4). Within the contemporary climate (1990-2020) average air temperatures are coldest February-March (avg. -12°C) and warmest in July (avg. 7°C). Temperatures rarely reach the extremes observed at similar latitudes; especially on the west coast of Spitsbergen which receives the bulk of the heat transported northward by the North Atlantic Current. Precipitation is frequent although light, with a noticeable drop in mean precipitation during April-June. The annual precipitation at Svalbard Lufthavn is less than half of what is measured at Barentsburg or Ny-Ålesund [Hanssen-Bauer et al., 2019] and as such it is not representative of the entire archipelago, or even the west coast of Spitsbergen. It is however relevant for our study area, the Foxfonna glacier system.

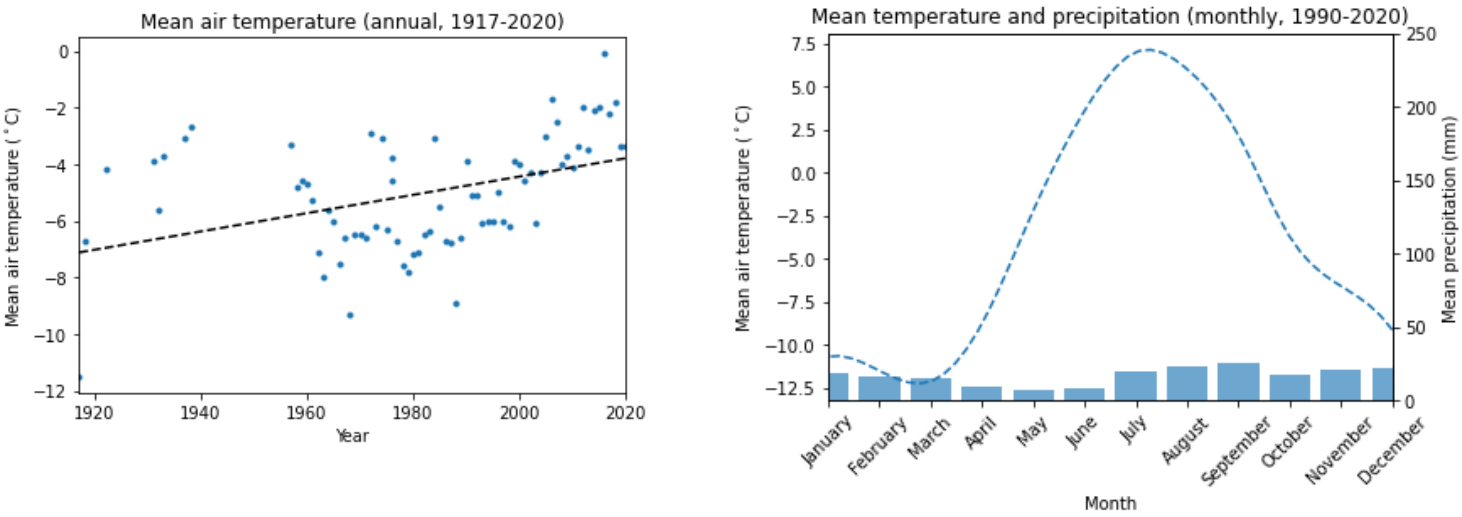

Figure 1.4: Mean annual air temperature observations at sea level (left), mean monthly precipitation and air temperature. Precipitation y-axis scaled to Bergen, Norway (60.3913°N, 5.3221°E) (right). Observations located on the coast of an inland fjord at Longyearbyen (SN99860) from 1917-1976; Svalbard Lufthavn (LYR, SN99840) from 1976-2020. A linear trend does not show the time-variability of climate change, but rather the change in mean temperature between two points in time [NKSS, 2021].

The climate of Svalbard has undergone major recent changes. In the past 1800 years summer temperatures have remained relatively stable while winter temperatures have fluctuated by an order of 5°C [D'Andrea et al., 2012]; specifically between two periods of rapid winter warming, situated at 800AD and the late 1800s - the latter warming period coming right after a cooling period known as the Little Ice Age (LIA) during which many glaciers were at their greatest Holocene extent.

The archipelago as a whole has experienced a warming trend since observations began in the early 1900s. Since the 1900s there has been a four-fold decadal increase in winter temperatures compared to summer temperatures (cf. 0.4 °C decade^{-1}, 0.1°C decade^{-1}) [Nordli et al., 2014]. The warming trend has been especially pronounced in the latter half of the 20th century. This, and other warming can be largely attributed to climate change and to the reduction of sea ice cover in the region [Divine and Dick, 2006]; this allows for more loss of heat from the relatively warm ocean to the atmosphere - the latter is a component to Arctic amplification [Kumar et al., 2010].

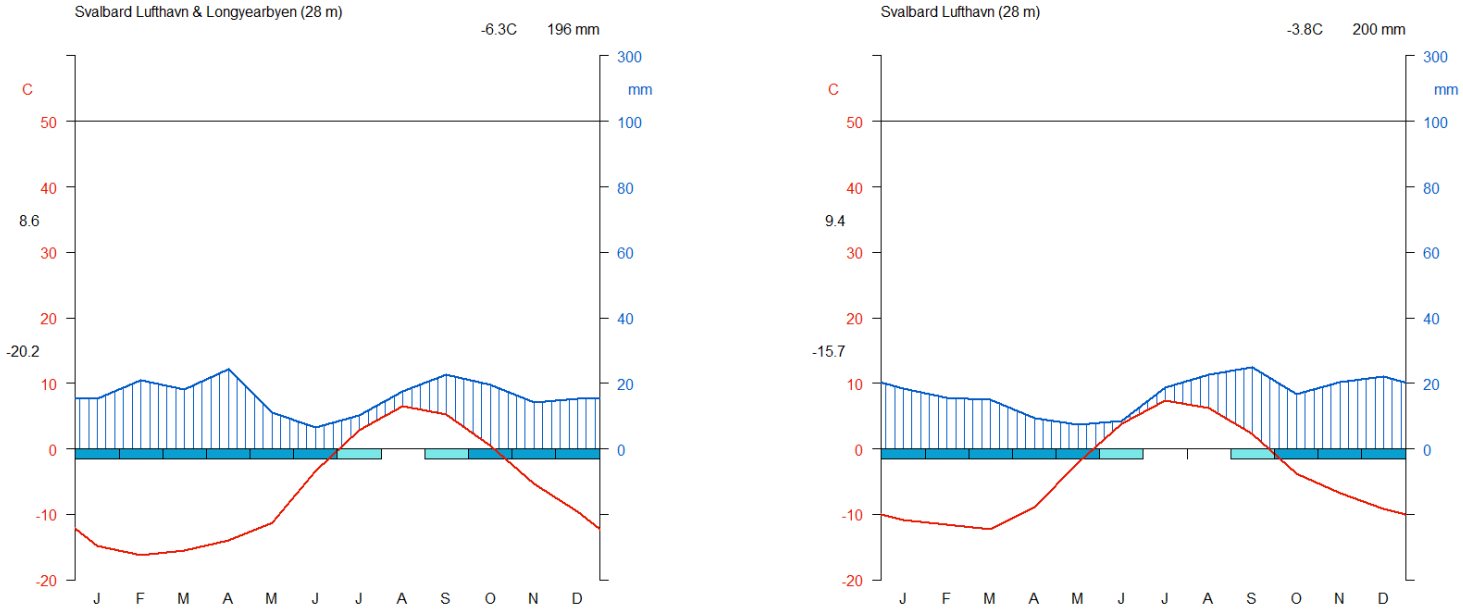

Figure 1.5: The local climate near Svalbard Lufthavn in 1960's and 2010's made by using 30-year climate averages collected from [NKSS, 2021]. A noticeable increase in surface air temperature has been recorded and the number of months with frost (dark blue bar) has decreased by one. Data shown includes: temperature (red curve), precipitation (blue curve).

Climate models project an 8°C increase in mean air temperatures by the end of the 21st century, while precipitation will increase by 50% relative to the 1971-2000 average [Hanssen-Bauer et al., 2019]. Due to Svalbard's relatively warm winter temperatures this increase in precipitation will not sufficiently aid glacier growth due to rain. Rather the change in climate will act as a substantial net negative to glacier mass and area [Hanssen-Bauer et al., 2019].

2. Theory

While some other processes are mentioned, this section primarily concerns land-terminating glaciers due to the chosen study area. Some core glacier knowledge and and terminology is covered, but the focus is on connecting the theory of glacier dynamics (i.e. Stokes equations) to the modelling software used (Elmer/Ice). Most of the information here has been derived from the books "The Physics of Glaciers" [Cuffey and Paterson, 2010], "Glaciers & Glaciation" [Benn D., 2010], and "Glaciers and Ice Sheets in the Climate System" [Fowler et al., 2019].

2.1 Drivers of glacier dynamics

Glaciers are perennial masses of ice on land which are driven to flow by the effects of gravity, and constrained by local topography; the flow of glaciers is effectively a case of a very viscous fluid deforming under its own weight. The growth and decline of glaciers is also largely dictated by the local climate, as any changes in mass, ice temperature, and rheology will affect the internal stresses the glacier is undergoing, and subsequently their flow. As such glaciers are heavily influenced by the contemporary, and past climate in the region.

2.1.1 Mass balance

Glaciers are in a constant state of exchange of mass and energy with the surrounding environment, the intensity of which varies with climatic conditions. Mass input occurs primarily through precipitation (e.g. snowfall) and the deposition of wind-transported snow onto the glacier. This input of mass is known as accumulation. Conversely mass output is known as ablation and primarily occurs via melting, or through calving - the latter is more common in sea-terminating glaciers. A single glacier can be divided into two zones depending on the accumulation and ablation patterns. Typically accumulation areas are located at higher elevations where the lower air temperatures - even in summertime - prevent snow melt from occurring. This results in a mass gain at higher elevations due to the retainment of a persistent year-round snow cover; over time this snow transforms into firn and glacier ice. Whereas the mass-losing ablation areas of a glacier are commonly located at a lower elevation where the mean annual air temperatures are much higher, thus prohibiting the year-round retention of a snow cover and promoting the melting of glacier ice and snow. Local topography can also affect the mass balance of a glacier, often altering the distribution of wind-transported snow, or via transporting mass to the glacier surface through snow avalanches from the adjacent mountainsides.

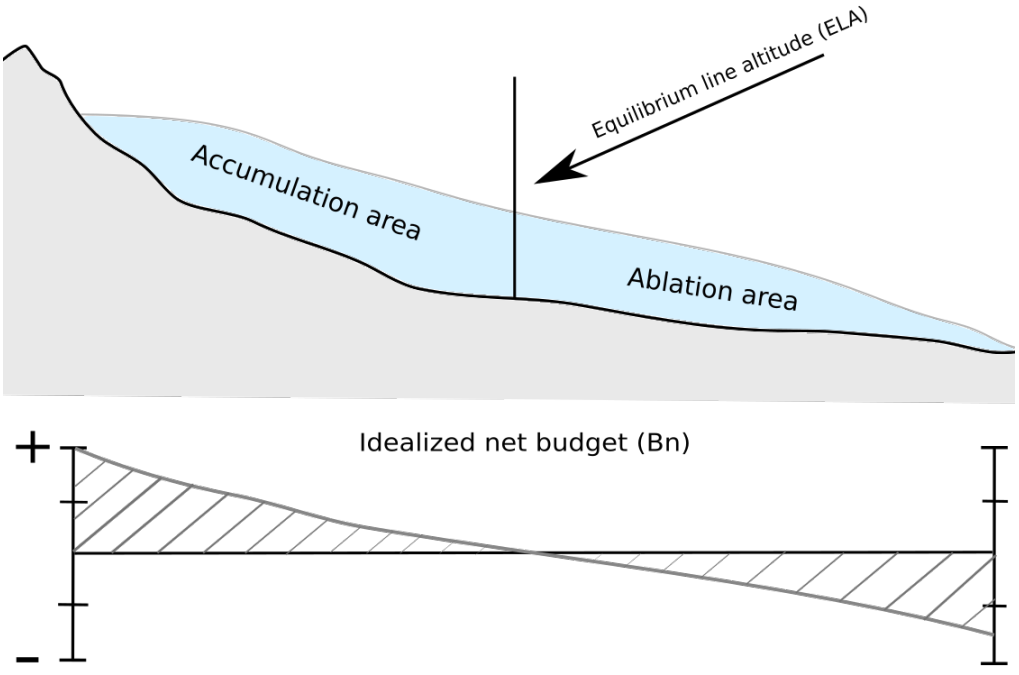

Figure 2.1: Idealized surface mass balance budget on a simple valley glacier. The accumulation area collects snow, resulting in a positive mass balance, while mass is lost in the ablation area due to e.g. melting. Overall the sum of the two, i.e. the net budget (Bn) is zero in an idealized steady state glacier.

Transfer of mass is an integral process in glaciers, as if it were non-existent the lower sections of a glacier would cease to exist after some time. In a stable climate the glaciers can reach a state of equilibrium, called steady state - where mass input matches mass output. This balance is what ultimately decides the extent and many characteristics of the glacier; changes in mass input at the top will alter flow velocities, affect ice thickness, and the pressure melting point at the bed. This will result in glaciers advancing or retreating over a long time-period for the rate of ablation to match that of accumulation.

2.1.2 Thermodynamics of glaciers

Temperature of glacier ice has a profound effect on the properties of ice and subsequently the dynamics of glaciers themselves. Energy is exchanged at the surface boundary via interaction with the atmosphere, and at the basal boundary due to the geothermal heat flux. The internal energy balance is affected further by four thermodynamic processes: (1) internal friction due to ice deformation, (2) friction from basal motion, (3) frictional heating due to water flow inside englacial water channels, (4) latent heat due to freezing or melting. Transport of energy within a glacier occurs largely by conduction due to diffusion of heat between individual grains of ice, by advection at the fluid-ice surface or by the flow of ice within the glacier.

Glaciers are often classified according to three sub-types, known as "thermal regimes", that depend on ice temperature: (a) cold-based glaciers which are below melting point throughout the glacier, (b) warm-based, temperate glaciers which are entirely at melting point, or (c) polythermal glaciers which are a mixture of the two. These definitions greatly influence the dynamics of a glacier. A cold-based glacier is frozen to its substrate and relatively immobile, whereas a temperate glacier will be lubricated by a thin sheet of water at its bed and able to move fast. It is important to note that the melting point of ice is only at 0°C when at atmospheric pressure and will decrease by 0.072 °C MPa^{-1} within glacier ice thus allowing for melt to occur at subzero temperatures. The effect equates to a e.g. pressure melting point of -0.64°C at the bed of a 1km thick glacier.

Near-surface ice temperature

Seasonal air temperature variations affect only the top 15 meters of ice below which ice temperature is ideally a representation of local climate, rather than weather (Figure 2.2). Changes to the surface ice temperature will take decades to occur if only due to temperature changes occurring in the local climate [Rabus and Echelmeyer, 2002]. Internal processes can infer faster changes to the glacier surface, such as (4) release of latent heat due to refreezing, which occurs due to percolating of water through the snow pack, which then refreezes at the glacier surface. The refreezing of 1g of water is able to warm 160g of snow or firn 1°C, thus warming the glacier. Whereas in the ablation area this refreezing will not occur due to the lack of a late season snow pack to refreeze within [Cai et al., 1986]; ablation area meltwater is "flushed" off the glacier over the barren ice. Due to this phenomena the glacier surface at a higher elevation can periodically be warmer than that of the rest of the glacier.

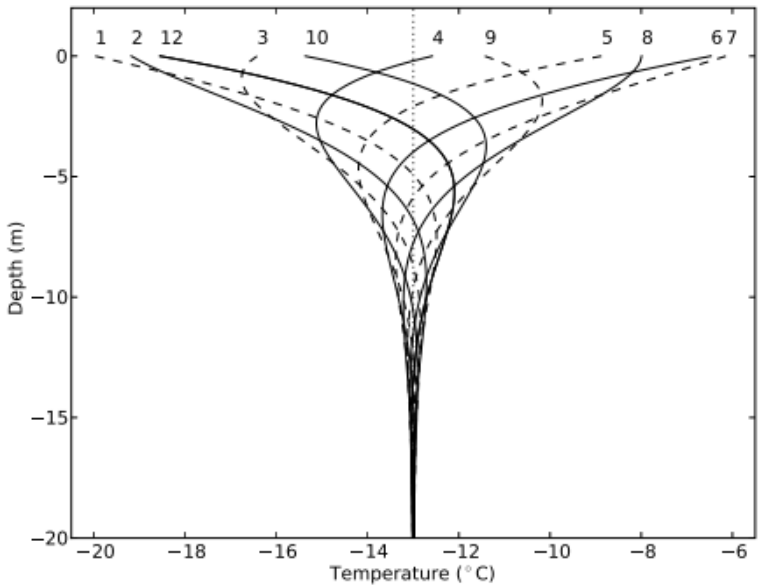

Figure 2.2: Temperature variations within the top 20 meters of glacier ice at the glacier Colle Gnifetti, Italy. Each numbered curve represents a month from 1 (January) to 12 (December). Odd numbered curves are dashed to improve readability [Haeberli et al., 1991]

2.1.3 Flow of glacier ice

The flow of glacier ice occurs primarily due to two processes, internal deformation and basal sliding. The internal stresses of a glacier refers to any height differences between two slabs of ice, which will cause a difference in hydrostatic pressure and create driving stresses that result in a down-slope flow of glacier ice - almost universally from the accumulation to the ablation areas (see Figure 2.1). This holds true both within a sloping geometry, e.g. mountain-based valley glaciers, as well as flat bedded ice caps; either the bed topography or the local precipitation patterns will instill an elevation difference within the ice field. Other factors such as climate and ice thickness will affect flow as well, as the viscosity of ice is temperature-dependent; warmer ice will flow faster than colder ice, as the colder will offer more resistance to deformation under applied stress due to higher viscosity. Deformation due to glacier flow results in the shearing, stretching, or otherwise distortion of the glacier due to the aforementioned internal stresses. The process of internal deformation is responsible for many of the well-known glacier surface features, such as lateral crevassing - particularly at the front of a tidewater glacier.

Another primary process of glacier flow is basal sliding (see also Section 2.2.5, "Sliding conditions"). This is the process of glacier ice sliding over its substrate, often due to a thin film of water developing between the two mediums or due to melt water penetration to parts of the glacier bed [Zwally et al., 2002]. Sliding provides substantial increases to ice flow velocities, however in cases where the glacier bed is not at pressure melting point (i.e. ice temperature at 0°C) the glacier will typically be frozen to its bed; thus in these circumstances sliding would only occur if melt water from external sources is able to be transported to the bed.

2.2 Governing Equations

2.2.1 Conservation of mass

Let's consider a fixed volume V, which we assign some mass to. The object is only allowed to exchange mass through the transport of material across its boundaries, i.e. mass is neither created or destroyed. This can be stated as

$$\frac{\partial}{\partial t}\int_V \rho dV = -\int_{\partial V} \rho \boldsymbol{u} \cdot \boldsymbol{n} dS = 0 \tag{2.1}$$

Where t is time, ρ is density, and dS is any path around the boundary. The $\mathbf{n}$ is the unit-length direction vector, pointing away from the object along the normal, and $\mathbf{u}$ is the velocity, $\mathbf{u}$(x,t). Following Gauss's divergence theorem and assuming that the solution must hold for any volume V, the solution can be stated simply as

$$\frac{\partial \rho}{\partial t} + \nabla \cdot (\rho \boldsymbol{u}) = 0 \tag{2.2}$$

A material such as glacier ice can be considered incompressible, or approximately so. Thus the density ρ is a constant allowing the previous equation to be simplified to

$$\nabla \cdot \boldsymbol{u} = 0 \tag{2.3}$$

stating that mass conservation requires a divergence-free velocity; this is known as the continuity equation.

2.2.2 Stress and strain rate

Cauchy stress tensor

To describe deformation under stress it is necessary to define the stress (i.e. the force per unit area) the material is subjected to. In continuum mechanics this can be achieved with the Cauchy, or total stress tensor $\boldsymbol{\sigma}$, which consists of nine components describing the stress an infinitesimally small cube of the material can be subjected to. In the Cartesian coordinate system this can be portrayed as

$$\boldsymbol{\sigma} = \sigma_{ij} = \begin{bmatrix} \sigma_{xx} & \sigma_{xy} & \sigma_{xz} \\ \sigma_{yx} & \sigma_{yy} & \sigma_{yz} \\ \sigma_{zx} & \sigma_{zy} & \sigma_{zz} \end{bmatrix} = \begin{bmatrix} \sigma_{x} & \tau_{xy} & \tau_{xz} \\ \tau_{yx} & \sigma_{y} & \tau_{yz} \\ \tau_{zx} & \tau_{zy} & \sigma_{z} \end{bmatrix} \tag{2.4}$$

where in the latter matrix the τ_{ni} represent the shear stresses acting parallel to the surface, and σ_n the normal stresses acting perpendicular to the surface of the material. The stress tensor can be visualized (Figure 2.3) as a infinitesimally small cube. Due to the infinitesimal nature of the cube, it has no moment of inertia of its own. Therefore the entire stress state can be described by six independent components of the Cauchy stress tensor $\boldsymbol{\sigma}$, namely $\sigma_{xx}, \sigma_{yy}, \sigma_{zz}, \sigma_{xy}, \sigma_{xz}, \sigma_{yz}$. The other components ($\sigma_{yx}, \sigma_{zx}, \sigma_{zy}$) are not independent, as they are symmetric with the components $\sigma_{xy}, \sigma_{xz}, \sigma_{yz}$, e.g. $\sigma_{ji} = \sigma_{ij}$ in a system which must remain in equilibrium. Thus only the aforementioned six entries of the stress tensor are necessary to describe the stress state.

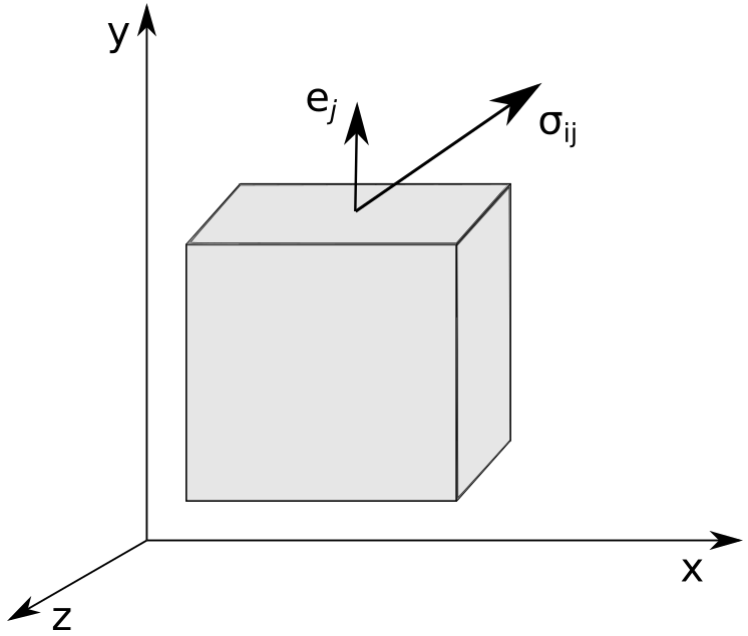

Figure 2.3: A cube representation of a single stress vector acting on a facet of material. Here the stress is acting on the jth face of the cube. The stress acting on an arbitrary surface is given by s = $\sigma_{ij}nj$, of which the above picture is a simplification.

By defining the negative means of all σ_{ii} components as pressure we can describe the total pressure on this cube as

$$p = -\frac{1}{3}\text{tr}\boldsymbol{\sigma} = -\frac{1}{3}(\sigma_{xx} + \sigma_{yy} + \sigma_{zz}) \tag{2.5}$$

where the negative sign due to convention, e.g. positive pressures act to compress on the cube. This is typically further decomposed into a form of the total stress tensor where the isotropic, i.e. pressure component, and the deviatoric stress are separate:

$$\sigma_{ij} = \tau_{ij} - p\delta_{ij} \tag{2.6}$$

where δ_{ij} is the identity tensor and τ_{ij} is commonly known as the deviatoric stress tensor.

Strain rate

The strain-rate describes the rate of change, or deformation of a material/fluid in reaction to applied stress. The study of this deformation is called rheology, wherein the strain rate tensor is defined as

$$\dot{\epsilon}_{ij} = \frac{1}{2}(\frac{\partial u_i}{\partial x_j} + \frac{\partial u_j}{\partial x_i}) \tag{2.7}$$

for which the sum of the above equation is zero in an incompressible material such as glacier ice. A deformation law gives the relationship between the deviatoric stress and strain-rate tensor,

$$\tau_{ij} = 2\eta\dot{\epsilon}_{ij} \tag{2.8}$$

where η is the effective viscosity.

2.2.3 Glen's flow law

Solving the stress-strain rate relationship for fluids with a varying viscosity requires different solution. In glaciology this has been described with

$$\dot{\epsilon}_{ij} = A(T)\tau_{ij}^{n-1}\tau_{ij} \quad , \quad \tau = \sqrt{\frac{1}{2}\tau_{ij}^2} \tag{2.9}$$

which is known as Glen's flow law. The power exponent n = 3, while *A(T)* is the temperature-dependent rate factor. This relation has been proven to hold water in typical glacier flows of 50-150kPa [Cuffey and Paterson, 2010]. By inserting (Equation 2.9) into (Equation 2.8), we get a different form for Glen's law

$$\tau = 2\eta A(T)\tau_{ij}^{n-1}\tau_{ij} \tag{2.10}$$

which we can solve to get the temperature-dependent effective viscosity η

$$\eta(T) = \frac{1}{2}(A(T)\tau_{ij}^{n-1})^{-1} \tag{2.11}$$

Multiplying Equation 2.9 (left) with itself and $\frac{1}{2}$ gives us

$$\frac{1}{2}\dot{\epsilon}_{ij}\dot{\epsilon}_{ij} = A(T)^2\tau^{2(n-1)}\frac{1}{2}\tau_{ij}\tau_{ij} \tag{2.12}$$

where the left-side term equals the effective strain rate and a portion of the right-side term equals the effective stress

$$\frac{1}{2}\dot{\epsilon}_{ij}\dot{\epsilon}_{ij} = \dot{\epsilon}^2 \quad , \quad \frac{1}{2}\tau_{ij}\tau_{ij} = \tau^2 \tag{2.13}$$

allowing us to relate terms

$$\dot{\epsilon} = A(T)\tau^n \tag{2.14}$$

Following the example set in [Greve and Blatter, 2009], pages 53-56, a non-linear solution for the effective viscosity (Equation 2.11) can be reached, which accounts for both ice temperature and effective strain rate,

$$\eta(T, \dot{\epsilon}) = \frac{1}{2}A(T)^{-1/n}\,(\dot{\epsilon})^{(1/n-1)} \tag{2.15}$$

Temperature dependency

The rate factor *A(T)* in Glen's flow law can vary by a factor of ~1000 over the range of temperatures (-55°C to 0°C) found in glaciers. The value of the rate factor can be described by the Arrhenius law

$$A = A_0 \exp(-\frac{Q}{RT}) \tag{2.16}$$

where Q is the activation energy, R is the ideal gas constant, and T is the temperature (in Kelvin).

Glen's enhancement factor

An enhancement factor (E) is often used in Glen's flow law, which allows for the multiplication of the rate factor to account for uncertainties outside the effects of stress or temperature; namely (ice) grain size, fabric, and impurities within the ice. A notable change in the recommended value for the enhancement factor occurs between Holocene and Ice-age ice, where it is noted that grain size between these layers of ice changes fast [Cuffey and Paterson, 2010]; grain size is smaller in Ice-age ice. It has been theorized [Koerner et al., 1979] that microparticles ($\varnothing$ avg. 0.3 μm) within the ice inhibit grain growth and boundary migration, thus creating softer, more malleable ice. However [Duval et al., 1980] found that the dispersion of impurities in the ice is not the greatest determinant of small grain size, rather the orientation of the grain c-axes within the fabric was more prominent.

Experiments both in the field and within controlled environments have provided for a range of values for E, namely [0.9-2.5] for Arctic Holocene ice, and [2-6] for Arctic Ice-age ice, with recommended values of 2 and 5 respectively [Cuffey and Paterson, 2010]. Nevertheless, the value of the enhancement factor should be fitted to observations without unreasonably diverging from previously observed and recommended values.

2.2.4 Stokes flow

For fluids where internal viscous and gravitational forces are substantially larger than inertial forces, the flow is best treated as Stokes flow, known also as creeping motion. It is a linearization of the Navier-Stokes equations and intended to be used in cases where the fluid is very viscous and slow moving, and as such is suitable in characterizing glacier flow. Starting with the Navier-Stokes equation,

$$\rho \frac{D\mathbf{u}}{Dt} = \rho g - \nabla p + \eta \nabla^2 \mathbf{u} \tag{2.17}$$

We have the inertial terms on the left hand side and viscous terms on the right hand side. When the flow is very viscous and slow - such as in Stokes flow - the inertial terms are negligible compared to the viscous and gravitational terms. We can assign the inertial term to equal zero on the left-hand side and insert (Equation 2.9) into the rightmost term. We are then left with reduced forms of the mass and momentum conservation laws (Equation 2.3),

$$\nabla \cdot \mathbf{u} = 0 \tag{2.18}$$

$$\rho \boldsymbol{g} - \nabla p + \nabla \cdot \boldsymbol{\tau} = 0 \tag{2.19}$$

which are the Stokes flow equations. The equations are time-independent but do depend on some parameters, such as temperature, and any given boundary conditions that are assigned to them.

2.2.5 Boundary conditions

Two kinds of boundary conditions are used in this thesis: (1) fixed boundary conditions - sometimes called Dirichlet boundary conditions - and (2) free boundary conditions. Under fixed boundary conditions we impose values on specific components (e.g. velocity, temperature) of the equation when at a predetermined boundary, such as the glacier bed or surface. For the free boundaries the solution is not described and needs to be solved for at the boundary.

No-slip and no-penetration conditions

A common solution to the flow of cold and polythermal glaciers is to prescribe a no-slip condition for the velocity at the bedrock, as well as a rigid bedrock allowing no penetration of the flow through the bed surface. These can be simply stated as

$$v_b = 0 \quad \text{and} \quad v_\perp = 0 \tag{2.20}$$

where v_b is the tangential velocity of the ice in relation to the bed with a direction downslope, while $v_\perp$ is the normal velocity at the bed, pointing upwards. The no-slip condition simply states that the ice is moving at the same velocity as the bed. Typically the bed is considered stationary, thus the ice is stationary as well

$$v_{bed} = v_b = 0 \tag{2.21}$$

Sliding conditions

The no-slip condition does not hold if the bed is at the melting point since in these conditions a thin layer of water can develop between the glacier ice and the bed, which will allow for sliding to occur. This movement can be described through a simple linear friction law which solves the basal shear stress as a function of sliding velocity,

$$\tau_b + \beta u_b = 0 \quad \text{or} \quad u_b + C\tau_b = 0 \tag{2.22}$$

or through more detailed non-linear laws. Here the β is the friction parameter, or slip coefficient, and C is the sliding parameter. This can be further solved for the relation between basal shear stress τ_b and the slip coefficient β,

$$\tau_b = -\beta u_b \tag{2.23}$$

A common friction law is the Weertman friction law. This law is suited for bed at pressure melting point, as it assumes that the bed and glacier are entirely separated by a 1μm thin sheet of water and that the bed is rough all around. Here the main resistance to the glacier flow is provided by the effects of regelation and enhanced creep. The former is the pressure melting and refreezing of ice against objects as it flows downslope, while the latter affects the stress-strain relationship of ice encountering objects in the flow path.

3. Data

3.1 Digital Elevation Models

Digital elevation models (DEMs) were used in the creation of the Elmer-compatible 3D mesh. The 1961, 1990, 2009 surface DEMs were created from aerial photography of the general area and digitized by Erik Schytt Holmlund using orthophotogrammetry as a part of his MSc thesis [Holmlund, 2020]. The 2004 DEM was provided by the Store Norske Spitsbergen Kulkompanie (SNSK), but with unreported details on the methods. The 2020 glacier surface DEM and 2021 ice thickness DEM were provided by [Cheung, 2021].

The 1961 surface DEM contains some interpolation due to missing data, known as "voids" [McNabb, 2018]; this method was primarily used on the slope between the ice cap and glacier. Other than that, there are no reported batches of missing data in the elevation models.

The resolution of the elevation models produced with photogrammetry is 10 m/px, meaning each pixel forms a 10x10 meter square on the DEM. The 2020 glacier surface DEM has a remarkably higher resolution of 0.25 m/px and the 2021 ice thickness DEM has a resolution of 3 m/px. For simplicity and to save on computational resources these higher resolutions were not utilized to their fullest; a 10x10 grid was used to pull data from the elevation models.

Bed topography was acquired by subtracting the glacier ice thickness of 2021 from a supplemented version of the 2020 surface DEM. The only change to the original surface DEM was the inclusion of the surrounding mountains - a necessary addition to satisfy the data format of Elmer/Ice. The elevation model for the thickness of the ice was provided by [Cheung, 2021].

The supplementing of the 2020 surface DEM was necessary, since the sampling grid covered an area larger than the DEM, thus creating points with null data and making it unreadable by Elmer. As the 2020 surface DEM covered both glaciers in their entirety, the only out-of-bounds data was in the surrounding mountains. In order to provide Elmer with a functional regular grid this out-of-bound data was supplemented with point elevation data from non-glaciated parts of the 1961 surface DEM. This was done using QGIS tools [QGIS, 2021], and was approached with two assumptions: (1) the glacier surface had shrunk, or at least remained the same since 1961 and as such the lower elevation values are all from the 2020 elevation model, (2) any data points not on the glacier will have the same elevation in 2020 as in 1961. Combining the 2020 and 1961 DEMs in this way allowed for the creation of a complete, but modified 2020 surface DEM of the glaciers and the surrounding mountains in a format readable by Elmer/Ice.

Elevation model	**Source of data**	**Resolution (m/px)**
1936 Surface	Aerial photography	50
1961 Surface	NPI Aerial photography	10
1990 Surface	NPI Aerial photography	10
2004 Surface	SNSK	5
2009 Surface	NPI Aerial photography	5
2020 Surface	UNIS Drone survey	0.25
2021 Bed	UNIS GPR survey	3

Table 3.1: Listed above are the different digital elevation models (ordered by year) used. Information on hte method of collection, resolution, and source is provided where possible. Aerial photography was digitized using orthophotogrammetry. Providers of the data: NPI (Norwegian Polar Institute), SNSK (Store Norske Spitsbergen Kulkompanie), UNIS (University Center in Svalbard).

3.2 Glaciology

Surface flow velocity

In situ velocity measurements of Foxfonna ice cap and glacier were conducted in 2012-2014 by [Koziol, 2014]. The data was collected by measuring the location of ablation stakes with a differential GPS (dGPS) and had a reported average horizontal accuracy of 0.035m (2012) and 0.018m (2014). No other data exists on the surface flow and due to undocumented relocation of the ablation stakes between 2014-2021 new measurements were impractical.

Stake	Velocity [m a^{-1}]		Velocity magnitude [m a^{-1}]	Vel. error [m a^{-1}]	Direction of movement
	Northward	Eastward			
FL1	-	-	-	-	-
FL2	2.023	-1.859	2.747	2.708 - 2.787	NW
FL3	0.297	-0.171	0.343	0.329 - 0.357	
FL4	-	-	-	-	-
FL5	1.991	-0.747	2.127	2.087 - 2.167	NNW
FL6	-	-	-	-	-
A AWS	-0.010	-0.019	0.021	0.008 - 0.035	W
A NE	-0.002	0.013	0.013	0.001 - 0.025	E
A N	0.193	-0.097	0.216	0.160 - 0.271	NNW
A NW	0.075	-0.026	0.080	0.042 - 0.117	N
A SW	-0.175	-0.232	0.290	0.261 - 0.320	SW
A SE	-0.624	-0.745	0.971	0.949 - 0.994	SW
A S1	-	-	-	-	-
A S2	-0.116	0.033	0.120	0.100 - 0.141	SSE

Table 3.2: Surface velocities observed on Foxfonna glacier and ice cap during 2012-2014 [Koziol, 2014]. Directions of positive velocity are towards the north and east. A total magnitude for the velocity is provided, as well as the geographic orientation of the velocity vector. The velocity error is provided by [Koziol, 2014], but the method it was calculated with remains unknown even after personal correspondence with the author.

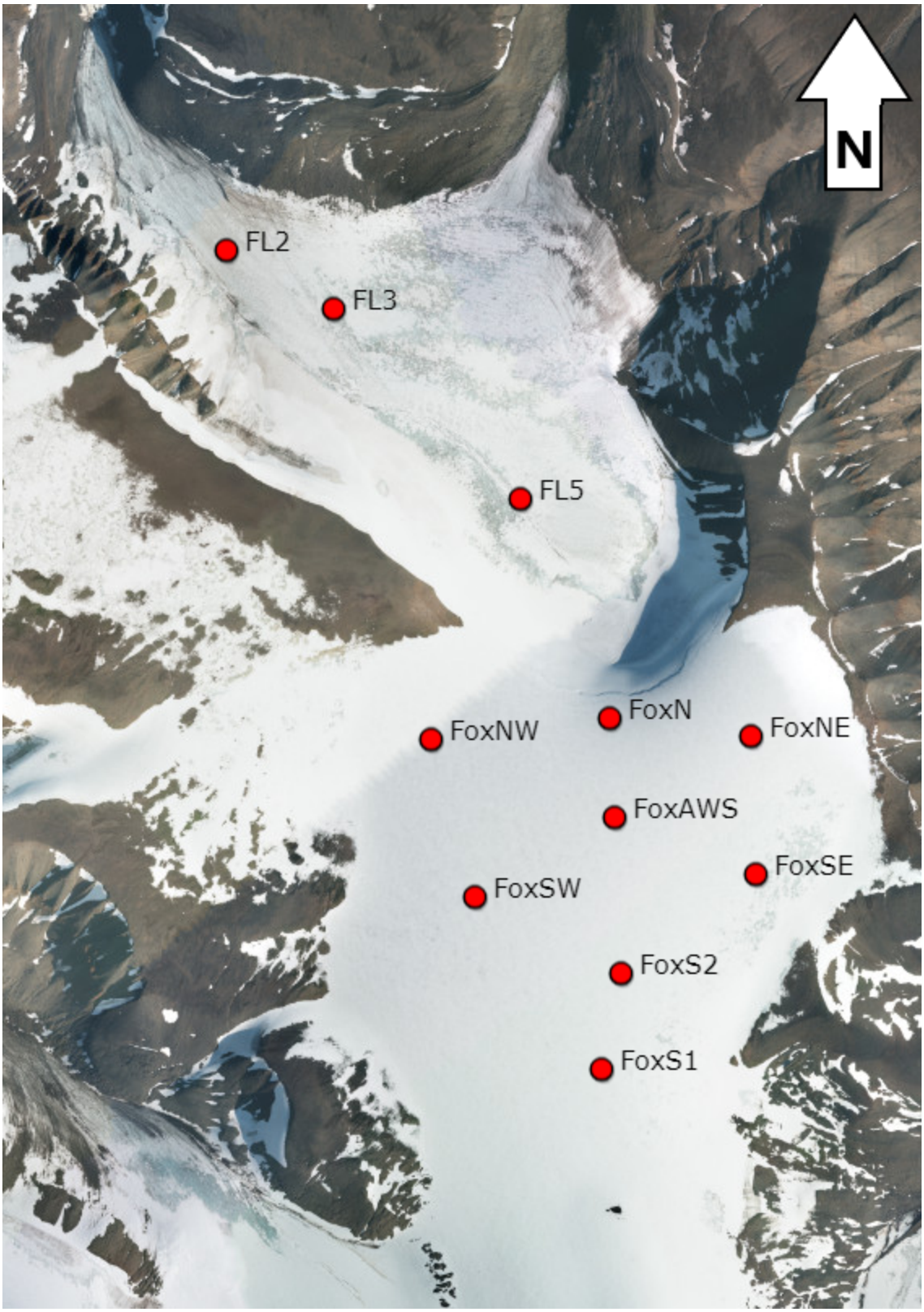

Figure 3.1: Satellite photo overlaid with the locations of ablation stakes (red dots) on Foxfonna. Only stakes where successful measurements for ice velocity were taken in 2012-2014 are included. Image courtesy of the Norwegian Polar Institute (https://toposvalbard.npolar.no/).

Ice, Bedrock and Permafrost Temperature

Temperatures within the Foxfonna glacier and at its bed are consistent with a cold-based glacier. Bed temperatures ranged from -3.3 to -3.4°C near the center (at 65m), while the glacier tongue was at -6.5°C (at 25m). Ice temperature near center, at halfway down to the bed was -4.4°C (see Figure 3.2). [Liestol, 1974].

Permafrost temperatures measured from the underlying mine shafts vary between -1.2°C to -4.9°C, with an extreme low of -5.8°C. The region underneath the Foxfonna glacier system, as well as the nearby environment, is a zone of continuous permafrost [Christiansen et al., 2005].

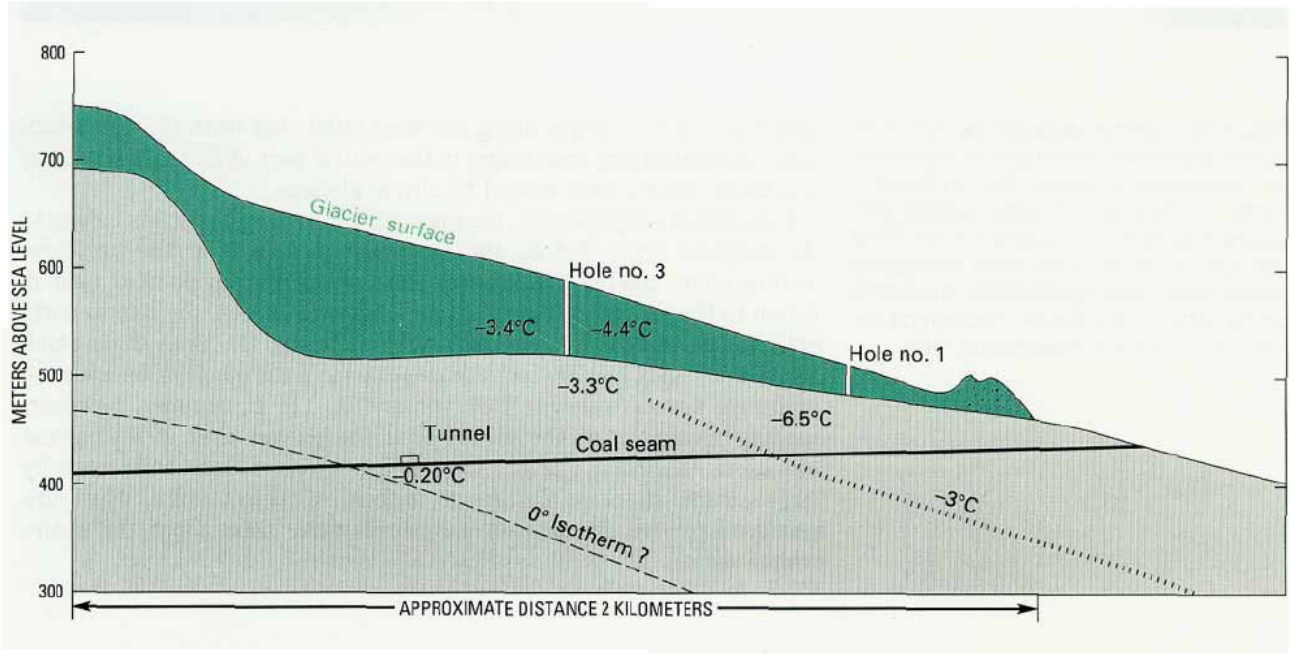

Figure 3.2: Glacier ice temperature of Foxfonna in the early 70's [Liestol, 1974] Borehole no. 1 is at 25 meters depth, borehole no.3 is at 65 meters depth. Both depths used in the measurement are deeper than the effect of seasonal variations. The ark green area denotes the glacier ice, light green area denotes the underlying surface. The 0°C and -3°C ground temperature isotherms are marked with a dashed and dotted line, respectively. The consistent dark line denotes the mine shaft below the glacier. Figure credit: U.S. Geological Survey [Liestol, 1993];

Surface Mass Balance

Two primary methods for surface mass balance were used in this thesis: glaciological and geodetic. Glaciological mass balance observations have been conducted consistently from 2007 to 2020 for the ice cap, see Figure 3.3, Table 3.3, [Rutter et al., 2011], [Koziol, 2014], [Hodson et al., 2020]. Foxfonna glacier has only been observed from 2010 to 2012 [Koziol, 2014], see Figure 3.4. The results for the geodetic mass balance are presented in Section 5, "Results".

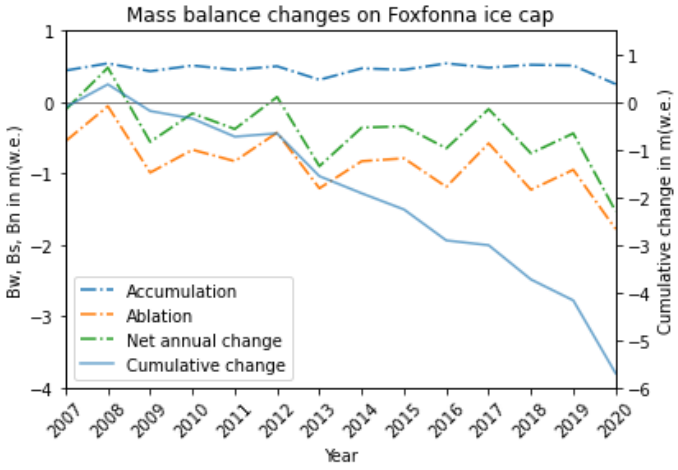

Figure 3.3: Foxfonna ice cap surface mass balance, 2007-2020 [Hodson et al., 2020]. Dashed lines denote the annual accumulation (blue), annual ablation (orange), net annual change (green).

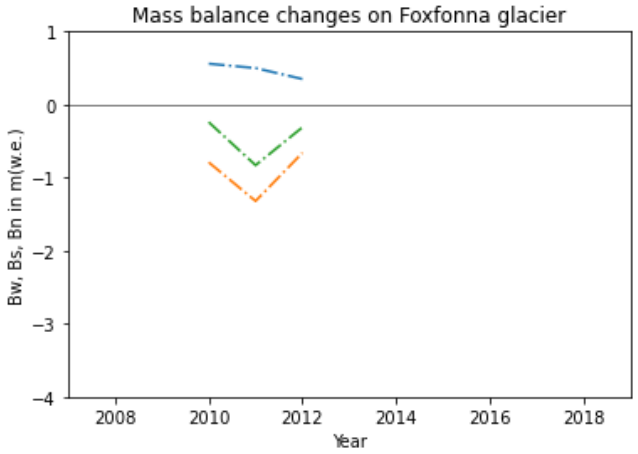

Figure 3.4: Foxfonna glacier surface mass balance, 2010-2012 [Koziol, 2014]. Dashed lines denote the annual accumulation (blue), annual ablation (orange), net annual change (green).

Bn m w.e.	2007	2008	2009	2010	2011	2012	2013	2014	2015	2016	2017	2018	2019	2020
Fox NW	0.06	0.48	-0.52	-0.14	-0.33	0.12	-0.98	-0.41	-0.371	-0.50	-0.08	-0.68	-0.33	-1.26
Fox SW	0.09	0.41	-0.51	-0.15	-0.32	0.04	-0.89	-0.38	-0.322	-0.76	-0.31	-0.87	-0.22	-1.49
Fox AWS	-0.06	0.70	-0.52	0.06	-0.17	0.12	-0.70	-0.28	-0.780	-0.26	0.18	-0.53	-0.45	-1.42
Fox N	0.19	0.77	-0.70	0.04	-0.07	0.20	-0.66	-0.07	0.066	-0.02	0.07	-0.57	-0.50	-1.58
Fox NE	-0.10	0.53	-0.39	-0.17	-0.27	0.26	-0.69	-0.13	-0.183	-0.60	0.02	-0.48	-0.29	-1.59
Fox SE	-0.65	0.26	-0.72	-0.50	-0.94	-0.15	-1.40	-0.62	-0.627	-1.14	-0.36	-1.00	-0.46	-1.69
Fox S1	-0.21	0.52	-0.54	-0.18	-0.76	-0.06	-1.05	-0.63	-0.199	-1.08	-0.05	-0.74	-0.58	-1.49
Fox S2	-0.19	0.14	-0.58	-0.20	-0.17	0.03	-0.80	-0.40	-0.301	-0.88	-0.24	-0.87	-0.68	-1.72

Table 3.3: Net accumulation (Bn) 2007-2020 on Foxfonna ice cap, provided in meters water equivalent (m w.e.). Negative values indicate mass loss, while positive values indicate mass gain [Hodson et al., 2020].

3.3 Meteorology

Meteorological and climate data was sourced from the Norwegian Centre for Climate Services [NKSS, 2021]. Data used included annual mean air temperature 1917-2020, monthly temperatures 1990-2020, monthly precipitation values 1990-2020, monthly mean maximum air temperature 1990-2020, monthly mean minimum air temperature 1990-2020, monthly minimum air temperature 1990-2020.

Data from 1917-1976 is from Longyearbyen (SN99860), and from 1976-2020 all data is sourced from Svalbard Lufthavn (SN99840), [78.246N, 15.493E]. Both stations were chosen due to their long running history of observations. All temperature values were in °C, and precipitation values in mm/month. The annual mean temperatures were used as a free surface boundary condition in the model after including the effect of altitude; the tropospheric lapse rate is around 4.5 °C/km at polar latitudes - much lower than the 6.5 °C/km closer to the equator [Stone et al., 1979], [Mokhov et al., 2006]. Other weather data was used in characterizing the local climate (see Figures 1.4, 1.5).

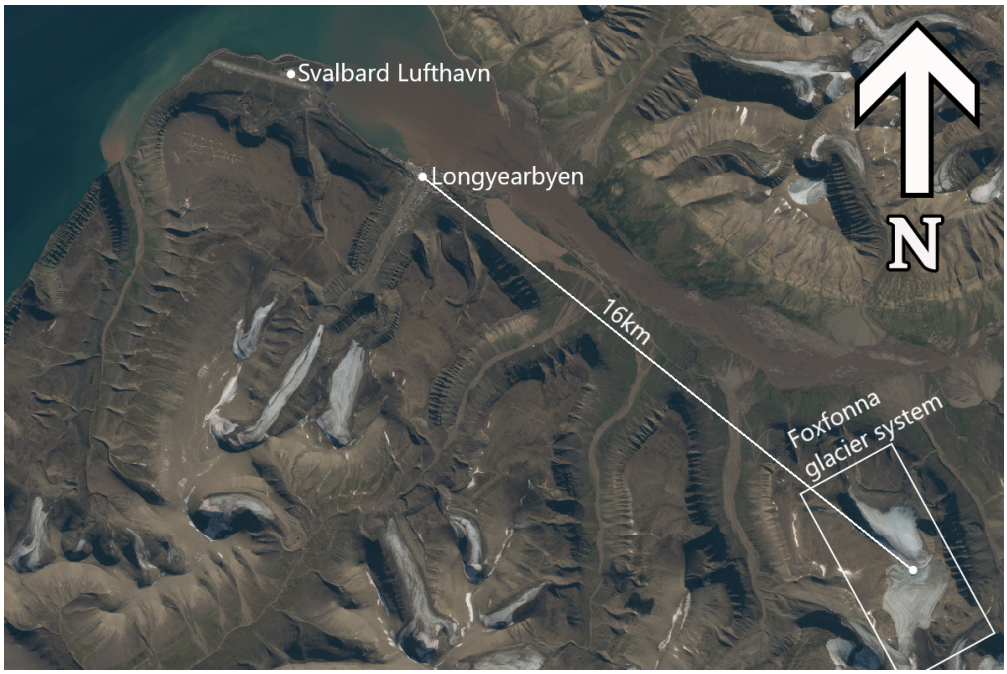

Figure 3.5: The approximate location of the two weather stations (at sea level) in relation to the Foxfonna glacier. Pictures: Adventdalen valley, with the locations of the Foxfonna glacier system, Longyearbyen, and Svalbard Airport (Lufthavn) included. Image courtesy of the Norwegian Polar Institute (https://toposvalbard.npolar.no/).

3.4 Supporting data and quality assessment of the DEMs

14C dating on organic samples

Undisturbed samples of moss (Pohlia sp., Pohlia obtusifolia) were discovered within 1.5 meters of the retreating glacier margin. 14C radiocarbon dating estimated their age at roughly 1500 years, see Table 3.4, [Roche, 2021].

Location	Elevation (m.a.s.l)	Median age (yr)	Error (+/-)
N78.13362, E16.20745	789	1480	59/68
N78.12963, E16.21327	758	1482	89/81
N78.13403, E16.20680	788	1463	62/68

Table 3.4: Results from a 14C carbon dating of moss at the retreating glacier margin of Foxfonna ice cap. All three samples were found undisturbed within 1.5 meters of the margin, from an area previously covered by the glacier.

Geothermal heat flux

The geothermal flux in the local area is 67 mW/m^2 [Isaksen et al., 2000]. The observed value was measured during a field campaign running from 1998-1999 on top of Janssonhaugen, roughly 6 kilometers from Foxfonna. A similar value of 70 mW/m^2 was measured nearby Longyearbyen [Betlem, 2018] a distance of 15 kilometers from Foxfonna.

Steepness of the free surface

The Foxfonna valley glacier is not very steep, and in general the slope angle is no larger than 8°-10° along most of the glacier in either the 2009 or 2020 DEM. This can be seen in Figure 3.6 and is corroborated by [Koziol, 2014]. A notable difference on the north-eastern tongue where angles of up to 21° can be identified in the elevation models. Three areas of interest have been highlighted, (1) the NW tongue, (2) the NE tongue, (3) the top of the valley glacier. There is no substantial (>1°) difference between 2009-2020, except for at the NE tongue (3) where melt has steepened the glacier.

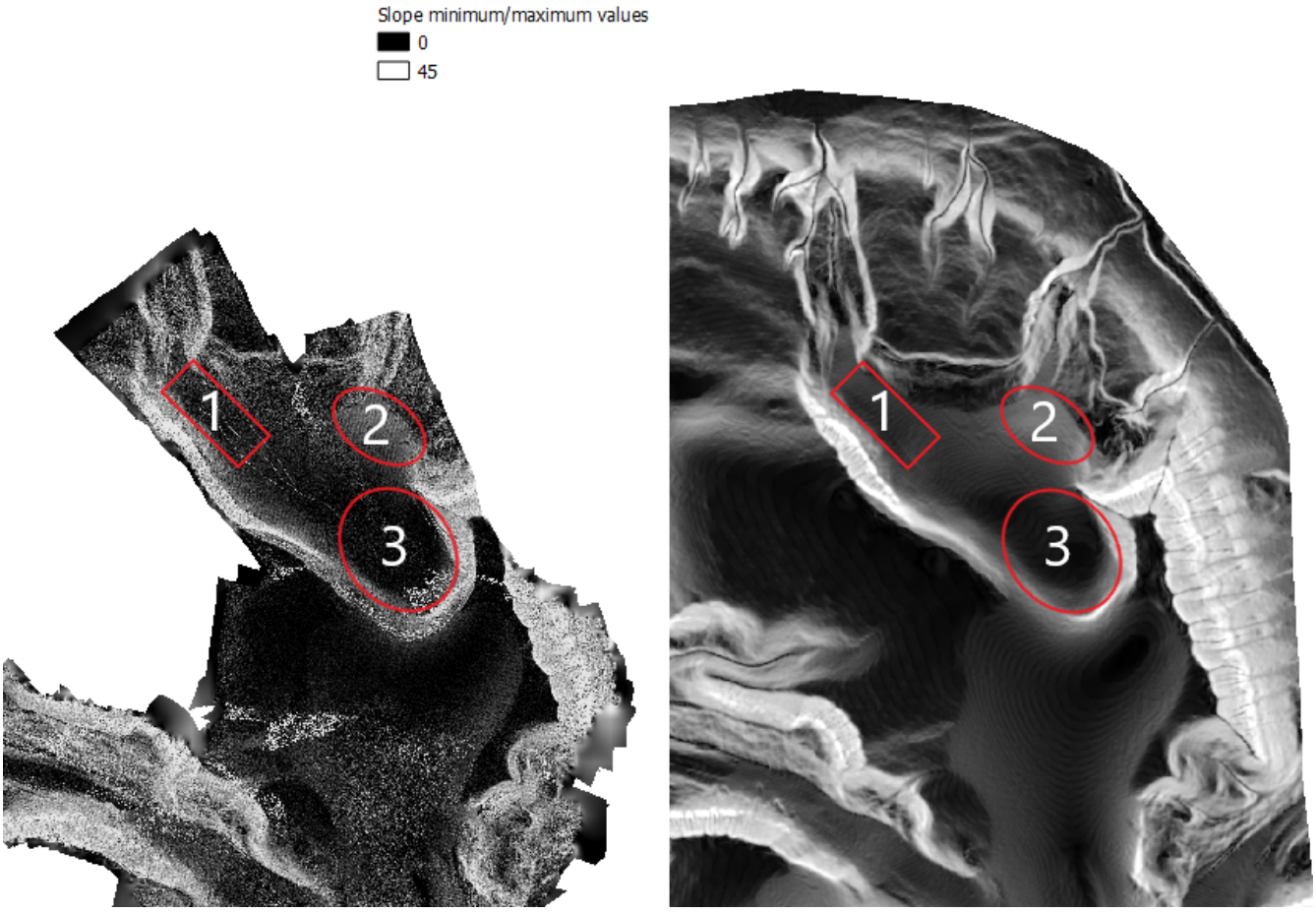

Figure 3.6: Slope angle (in degrees) of the Foxfonna valley glacier during 2020 (left) and 2009 (right), provided as an approximate presentation. Darker areas are flatter, while whiter areas are steeper. The slope angle of the three numbered regions ranges from (1) 6°-10°, (2) 9°-21°, (3) 1°-5° in both the 2020 DEM and 2009 DEM.

Ground penetrating radar (GPR)

GPR was used in April 2021 to acquire ice thickness over the glaciers. Subtracting the measured thickness of the ice from the 2020 glacier surface DEM allowed for solving the bed elevation in m.a.s.l. A comparison was done between depths given at overlapping transects and the percentual difference is shown in Figure 3.7. Larger differences - i.e. errors - can be seen on Foxfonna glacier. This is claimed to have been due to a higher reflectivity in the medium which impacted post-processing. This could be due to e.g. water near or at the bed, or temperate ice [Koziol, 2014], [Cheung, 2021].

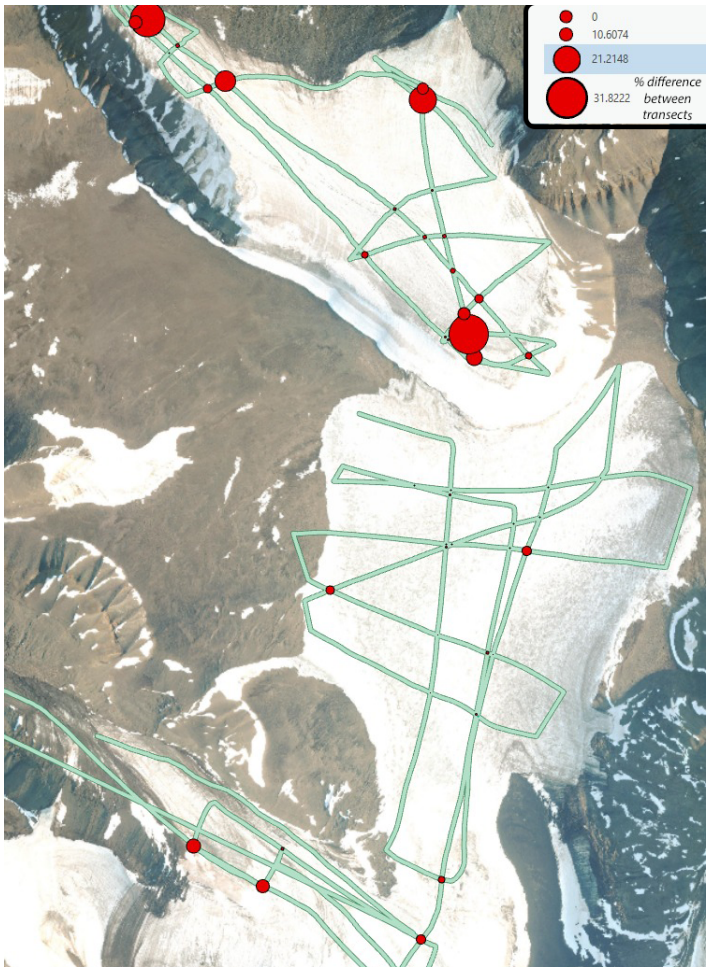

Figure 3.7: Transects made with ground-penetrating radar (in teal) during [Cheung, 2021] survey. At some overlapping transects a percentage difference between the two observations was calculated. These locations are marked by a red dot and the size of the red dot indicates the magnitude of the difference between the two observations.

3.4.1 Quality of the elevation models

The quality of the used elevation models is important for the accuracy of the model results. The only known structural issue is in the 2020 elevation model, which suffers from issues relating to the Structure from Motion method; the accuracy of the method degrades near the edges of the surveyed area due to the lack of photographs taken at multiple angles. There is no documentation following the elevation models from 1961, 1990, 2004, 2009 available to use in order to know if these elevation models suffered from some quality issue.

A simple method was used in order to compare the elevation models with each other: three non-glaciated points in time were selected and compared with each other. The elevation model from 2009 was chosen as a reference due to it being the most recent with a good resolution and no issues pertaining to the method. Points chosen included (in WGS84/UTM 33N) Point 1 [527600, 8674125], Point 2 [525885, 8675582], and Point 3 [525890, 8673520]. This comparison is useful in order to verify the precision of all models to each other. The precision of all the models with each other is in general good (see Table 3.5) - even across differing methods. This suggests that each model used is rather accurate to the true topography of the ice surface along the Foxfonna glacier system.

Location	Elevation (2009)	Deviation from 2009 DEM			
		2020	2004	1990	1961
Point 1	785.913	0.05%	0.09%	0.05%	0.04%
Point 2	449.988	3.7%	0.003%	-0.017%	-0.139%
Point 3	710.014	0.09%	-0.14%	-0.106 %	0.09%

Table 3.5: Percentage of deviation from the 2009 DEM. In general the elevation models are consistent with each other, with a sub-0.2% deviation, save for one chosen location in the 2020 elevation model. This deviation is likely due to the point being in an area poorly covered by the SfM method used in 2020.

Elevation model from 1936

The DEM of 1936 was not used in this project although it was made available. This is due to the models poor resolution, poor accuracy, and difficulty in using in Elmer/Ice. The most notable issue was that the ice cap in the 1961 model is thicker than the glacier of 1936 (see Figure 3.8), while a decline in glacier thickness is expected. This error may be due to optical issues when the original photograph was taken - such as cloudy weather - or an issue in the post-processing of the elevation model. Visible in the same figure is the pockmarked surface of the 1936 glacier - this may be due to an unknown failure in the method used to produce the elevation model.

Figure 3.8: The 1936 DEM (dark-grey) overlaid on the 1961 DEM (light-grey). The ice of the 1936 glacier is thicker in the valley glacier, but not thicker on most of the ice cap where a similar result would be expected. This is likely due to an error or failure in the method (photogrammetry).

4. Methods

The numerical simulations in this thesis were produced with Elmer/Ice, an open source Finite Element Method (FEM) software. The software solves the thermo-mechanically coupled flow while taking all stress components into account i.e. solving the Stokes problem of the flow. The basic function of Elmer/Ice and the solvers used in this thesis have been detailed in Section 4.2, "Elmer/Ice: finite element model".

4.1 Pre-processing of domain geometry and meshing

Digital elevation models of the bed and surface topography, as well as a 2D footprint of the glacier were used in the creation of the final 3D mesh. The first two acted as inputs to the interpolation of the glacier elevation(s), while the two-dimensional footprint was used to constrain the relevant area from the two DEMs for meshing. The footprint itself is a hand-drawn polygon created in QGIS around the 1961 extent of the glaciers.

Due to the nature of the hand-drawing process its accuracy and extent is subject to the authors interpretation of 1961 aerial photography. Pre-simulation the footprint was converted into a 2D finite element mesh using the included tool, named "Gmsh" [Geuzaine and Remacle, 2009], and further processed into an Elmer readable format using the built-in ElmerGrid tool. The resulting mesh was then extruded according to input DEMs using the built-in solvers "Grid2DInterpolator" and "StructuredMeshMapper" while running the simulation. More information on the solvers can be found in the Elmer Models manual and at the wiki http://elmerfem.org/elmerice/wiki/doku.php.

4.2 Elmer/Ice: finite element model

The numerical simulations within this thesis have been produced within Elmer/Ice, an open source Finite Element Method (FEM) code (http://elmerice.elmerfem.org/). Elmer/Ice is a full-Stokes model for ice flow, e.g. it is able to take into account all individual stress components (see Chapter 2.2, "Governing Equations"), [Gagliardini et al., 2013].

The method used is known as finite element analysis, a numerical method in which relevant differential equations are solved within a given 1D to 3D space. This space is known as the domain, and it is a complete mesh structure of the larger problem at hand (e.g. a glacier). The mesh is subdivided spatially into what are known as finite elements which are solved for numerically. The simulations can be run in either a (1) diagnostic, or steady state method, or a (2) prognostic, or time-transient method.

Elmer/Ice depends on so-called "solvers" to run the simulation in the way desired by the user. These vary from the full-Stokes solver to ones more specific to hydrology, calving, thermodynamics and more. In this thesis the following solvers were used: Navier-Stokes, DeformationalHeat, HeightDepth, TemperateIceSolver, ComputeNormal, EmergenceVelocity, ParticleAdvector, [Råback et al., 2022].

Elmer/Ice has been proven as a versatile tool in glaciological modelling. In relation to this thesis it has seen relevant use in the following publications: [Zwinger et al., 2009], [Zwinger et al., 2014], [Välisuo et al., 2017], [Compagno et al., 2019] where the age-of-ice or surface mass balance was modelled either as a main scientific goal, or in support of the main task.

Parallel computation

The domain was subdivided into four partitions within ElmerGrid using a tool called "Metis" [Karypis and Kumar, 1999] to use four CPU cores in order to solve the computational problems faster. Metis is a part of ElmerGrid and was used instead of a simpler geometric partition method due to its better performance with complex geometries; partitions made by Metis typically have fewer partition-partition boundaries.

4.3 Isochrone distribution

The age of the ice is solved for by placing a particle at each node in the mesh and transporting the particle back in time - a so-called Semi-Lagrangian method. The particle is advected backwards until it exits the glacier, at which point the time it took the particle to travel from its initial node to the exit will be assigned to the initial node.

This can be represented mathematically: say that the velocity field within the glacier is $\vec{v}$ and the travel time of the particle is $-\delta t$ and its origin is $\vec{r}_0$

$$\vec{r} = \vec{r}_0 + \int_0^{-\delta t} \vec{v} dt \tag{4.1}$$

when $\vec{r}$ no longer resides inside the glacier, the δt value for the travel time will be assigned to the initial node.

4.4 Surface mass balance

The method used is identical to that of [Välisuo et al., 2017] and presented here in short. By taking two consecutive surface elevation models we solve for their average surface elevation distribution using the arithmetic mean of each position (x,y). The elevation models separated in time can be called h_{t_1} and h_{t_2}, thus their arithmetic mean is

$$h_{t_1 \longrightarrow t_2} = \frac{1}{2}[h_{t1}(x,y) + h_{t2}(x,y)] \tag{4.2}$$

If we assume a linear change in the free surface between the two elevation models, then it must follow that

$$\frac{\partial h_{t_1 \longrightarrow t_2}}{\partial t} \approx \frac{h_{t2}(x,y) - h_{t1}(x,y)}{t_2 - t_1} \tag{4.3}$$

From [Greve and Blatter, 2009] we find that the kinematic boundary condition can be written as

$$\frac{\partial h}{\partial t} + u_h \frac{\partial h}{\partial x} + v_h \frac{\partial h}{\partial y} - w_h = a_\perp \tag{4.4}$$

The first term can be approximated with equation 4.3. The rest of the terms are calculated by the steady state simulation of the ice flow under the average geometry of two consecutive elevation models, i.e. the geometry is that of $h_{t_1 \longrightarrow t_2}$. The solution to the accumulation and ablation can then be expressed as

$$a_\perp^{(h_t 1 \longrightarrow h_t 2)} = \frac{\partial h_{t1 \longrightarrow t2}}{\partial t} - \vec{u}_{em}(h_{t_1 \longrightarrow t_2}, \vec{u}) \tag{4.5}$$

where $\vec{u}_{em}$ is the vertical glacier-flow velocity at the free surface (positive upwards). This equation allows us to solve for the average surface mass balance between the two points in time.

5. Results

5.1 Simulations

The results used to (1) verify the simulations and support the overall characterization of the glacier will be presented first in this chapter, followed by the results of the two primary simulations, (2) isochrone distribution, (3) surface mass balance change. The primary simulations were chosen for different reasons, (2) was chosen to provide unique insight into the modelled age distribution of the ice, while (3) was chosen due to the prevalence of mass balance studies on the glacier, allowing the comparison of modelled values to existing measurements. The in situ values are shown in figures and tables found within Section 3, "Data". Results for both glaciers will be discussed, but the focus will be on the upper Foxfonna ice cap. Each full-scale simulation is laid over the simulation domain and are oriented north-south, top-down. The simulation domain is a rough representation of the 1961 glacier extent and is represented by a grey-white background. Units are in meters per year (m/a) or meters (m), and Kelvin (K) - unless otherwise specified.

Ice creep constants	For (1) above and (2) below -10°C		Other constants	
Rate factor 1:	$2.89165 \cdot 10^{-13}$ MPa^{-3} a^{-1}		Ice density	917 kg m^{-3}
Rate factor 2	$2.42736 \cdot 10^{-2}$ MPa^{-3} a^{-1}		Glen's enhancement	1
Activation energy 1:	$60 \cdot 10^3$ J		Air temperature	267.6K
Activation energy 2:	$115 \cdot 10^3$ J		Geothermal flux	67 mW/m^2

Table 5.1: Model parameters and constants which are common between all simulations

Ice thickness

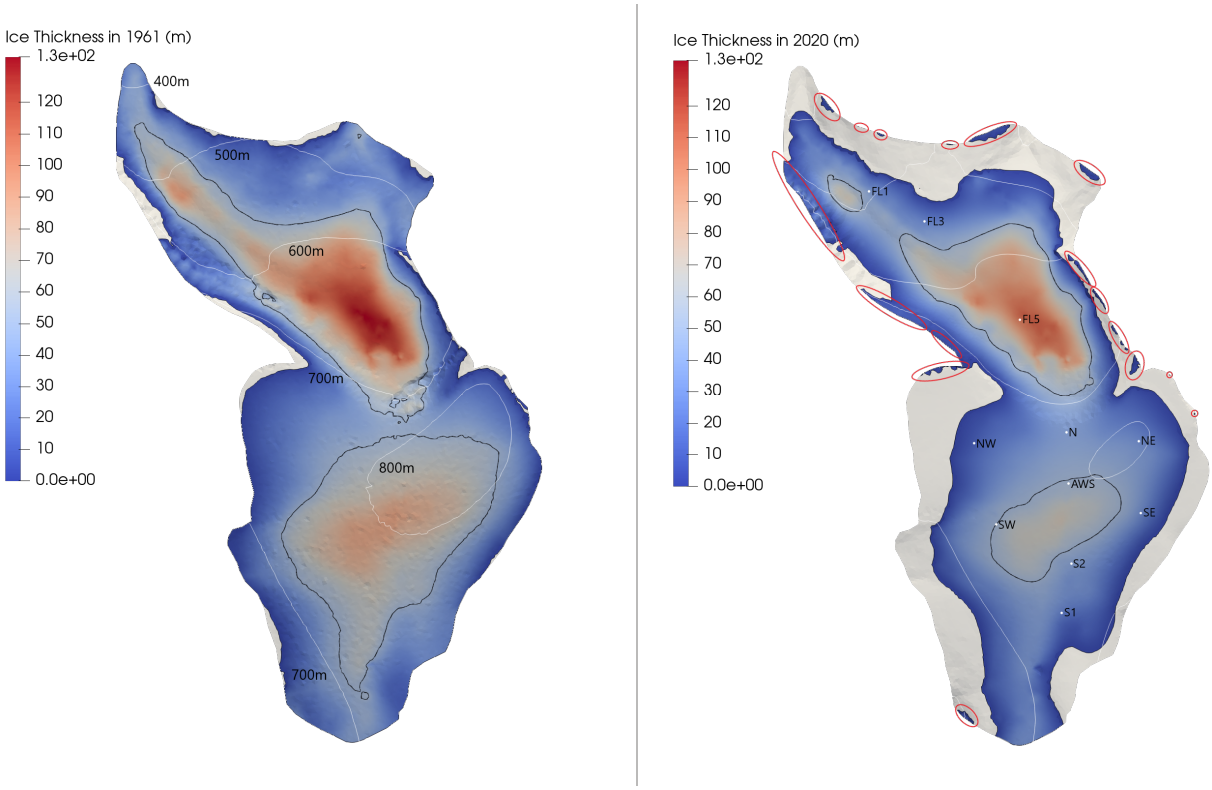

Figure 5.1: Total ice thickness (in meters) of the Foxfonna glacier system during 1961 and 2020. Glacier extent is defined by the 2 meter ice thickness limit and is overlaid upon the simulation domain (grey-white background). The white isoline represents the surface elevation in steps of 100 meters. The single black isoline represents 50 meter glacier thickness. Point FL2 is erroneously marked as FL1 in this figure.

Total ice thickness is a product of the basal elevation model combined with the free surface elevation model for its respective year. In general the ice thickness of both the upper and lower glacier has decreased around 10-20 meters between 1961-2020. The 2020 simulation has been highlighted with the geographic locations of 8 "permanent" ablation stakes in use since 2007 [Hodson et al., 2020], as well as the 3 temporary ablation stakes used in [Koziol, 2014] which have associated glacier flow velocity and mass balance data from 2011-2013. Both figures include a black isoline to represent where the glacier is 50 meters thick - this is to better visualize how the core area of the glacier has changed in time. Parts of the 2020 elevation model have been highlighted in red to indicate quality issues, which are discussed later.

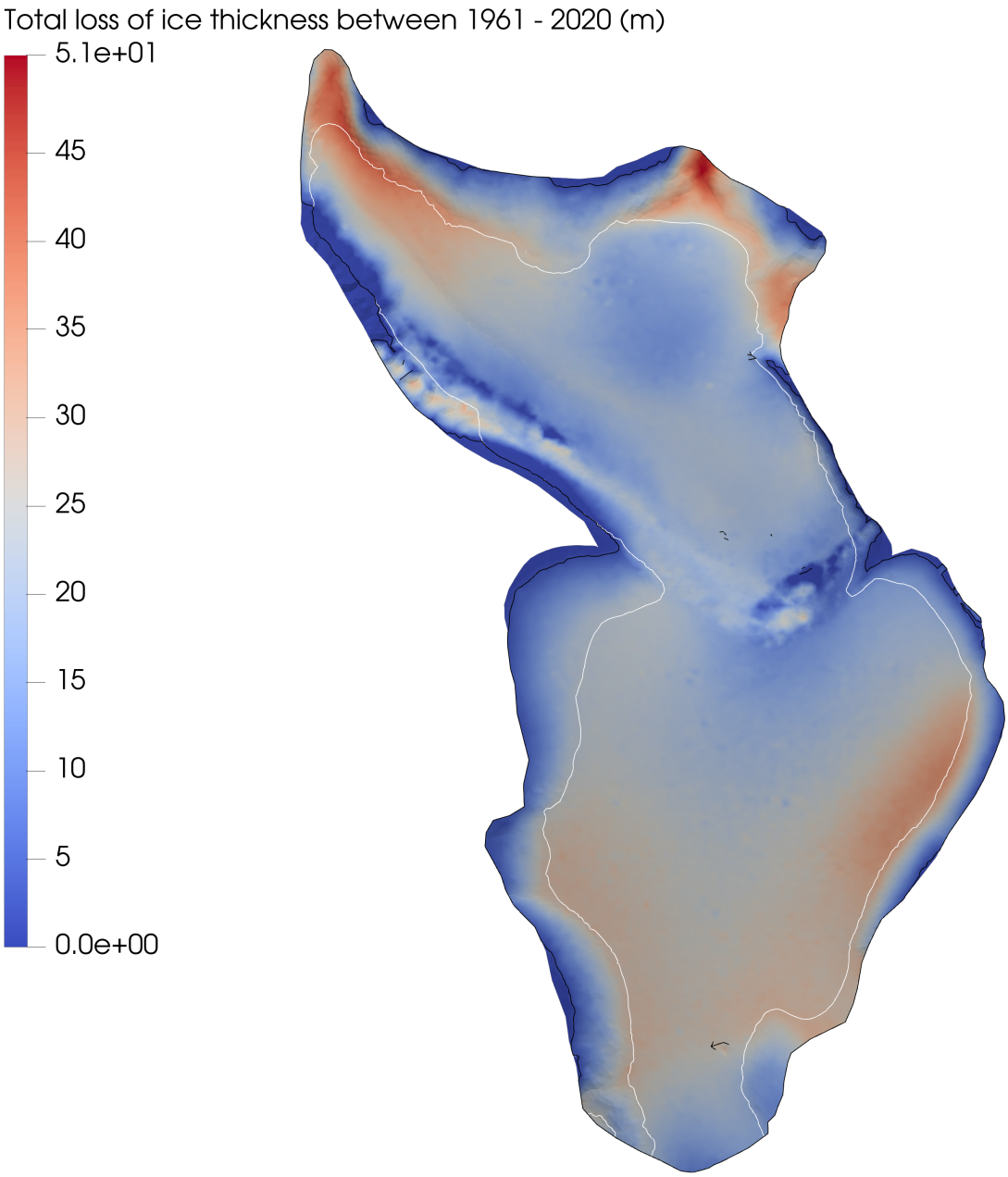

Figure 5.2: Total loss of ice of the Foxfonna glacier system between the years of 1961-2020 (in meters). Areas colored in red indicate a larger loss of ice, while blue areas indicated a smaller loss of ice. A thin black line represents the glacier extent of 1961, while a thin white line represents that of 2020. Between these two years nearly all sections of the glacier have experienced melt. Dark blue areas at the glacier margin likely indicate a lack of glaciation, rather than a section of the glacier surface with no loss of ice.

Ice flow velocity

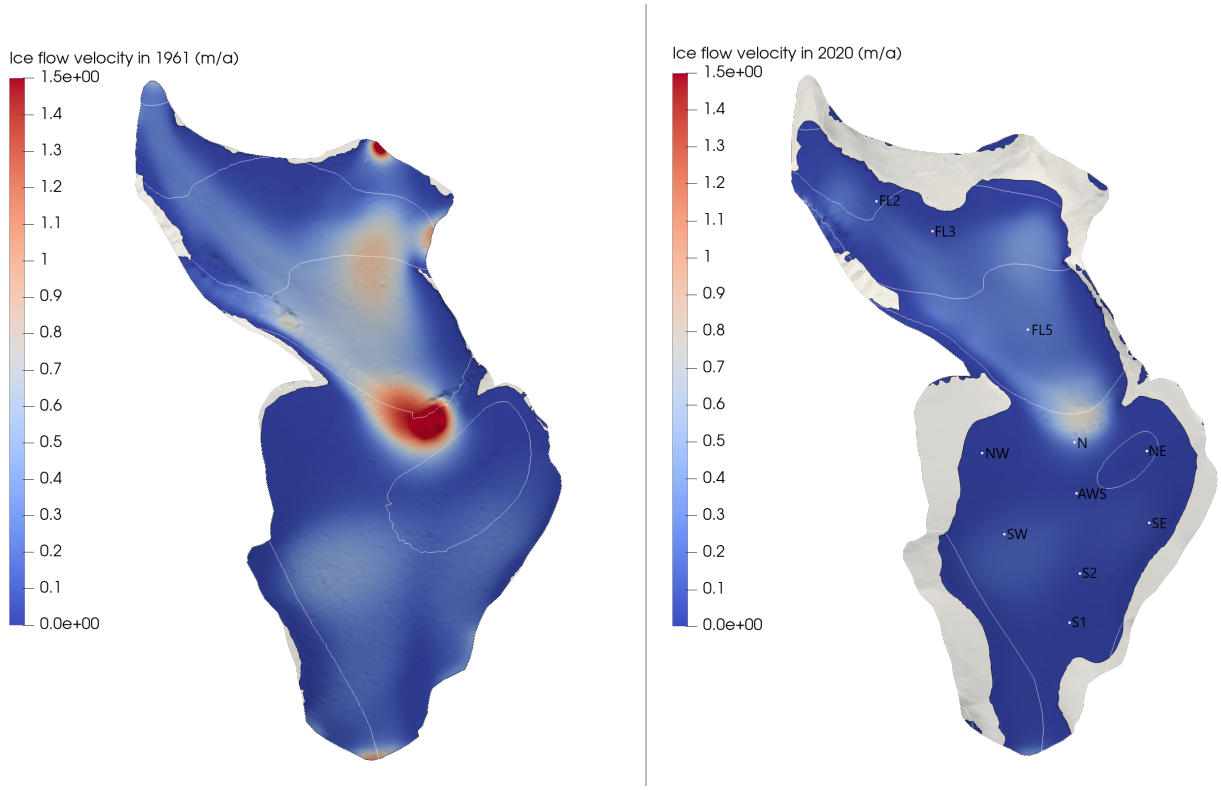

Figure 5.3: Ice flow velocities at the free surface of the Foxfonna glacier system in 1961 and 2020 (in m/a). The common scale of the units (0 - 1.5 m/a) was chosen in order to provide comparison and more color-contrast to the majority of the glacier. The white isoline represents the surface elevation in steps of 100 meters. The highest simulated velocity is on the crevassed slope between the upper and lower Foxfonna, which in 1961 flows at 2.2 m/a

The velocity of the glacier ice was simulated both for 1961 and 2020. The magnitude of the surface ice velocity can be seen in Figure 5.3, while the individual components for the 2020 simulation are presented in Figures 5.4, and 5.5. The scaling of 0 - 1.5 m/a and negative 0.25 m/a to positive 0.25 m/a was chosen to provide better contrast onto the slower velocities on the glacier, while still highlighting regions with faster flowing ice in a dark shade of blue (slower) or red (faster). All these figures are oriented north-south, top-down. The simulation of Foxfonna in 2020 includes some errors on the edges due to the field method used to collect the elevation model. These problem areas are highlighted in Figure 5.1 (right-side) and discussed further in Section 3.4.1, "Quality of the elevation models".

Stake	Simulated velocity [m a^{-1}]		Observed velocity [m a^{-1}]	
	x-component	y-component	x-component	y-component
SW	-0.089	-0.051	-0.232	-0.175
SE	0.028	-0.030	-0.745	-0.624
S2	0.0025	-0.025	0.033	-0.166
AWS	-0.013	-0.014	-0.019	-0.01
N	-0.095	0.316	-0.097	0.193
NE	0.0018	-0.0015	0.013	-0.002
NW	-0.0002	-0.00012	-0.026	0.0075
FL2	-0.033	0.047	-1.859	2.023
FL3	-0.025	0.045	-0.171	0.297
FL5	-0.1	0.19	-0.747	1.991

Table 5.2: A comparison of the simulated and observed glacier surface ice velocities (in meters per year) at each stake. The x-component is positive towards the east, the y-component is positive towards the north.

Table 5.2 (above) is a comparison of the simulation with a Glen's E of 1 and the observed velocities [Koziol, 2014]. Stakes SW, SE, S2, AWS, N, NE, NW are situated on the ice cap. Stakes FL2, FL3, FL5 are situated on the valley glacier. Observations are missing from stakes S1, FL1, FL4, FL6 and as such no simulation results for these stakes are given. A larger enhancement value would multiply each simulated x- and y-component value by the number of the enhancement value, e.g. an enhancement of 2 would double all x- and y-component values for these simulated results.

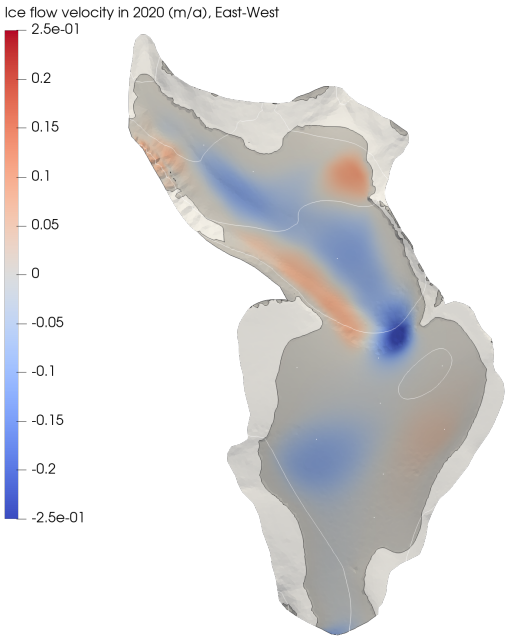

Figure 5.4: Flow of ice on the East-West axis on a 2020 steady-state simulation. A positive (red) value indicates eastern flow, while a negative (blue) indicates ice flow towards the west. The white isoline represents the surface elevation in steps of 100 meters.

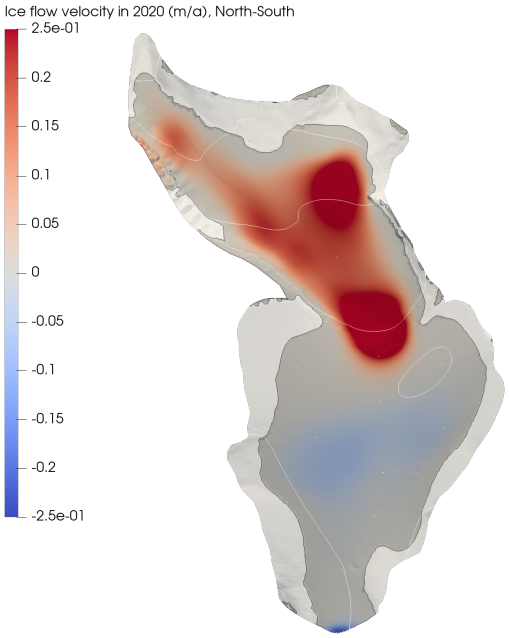

Figure 5.5: Flow of ice on the North-South axis on a 2020 steady-state simulation. A positive (red) value indicates northern flow, while a negative (blue) indicates ice flow towards the south. The white isoline represents the surface elevation in steps of 100 meters.

Ice temperature

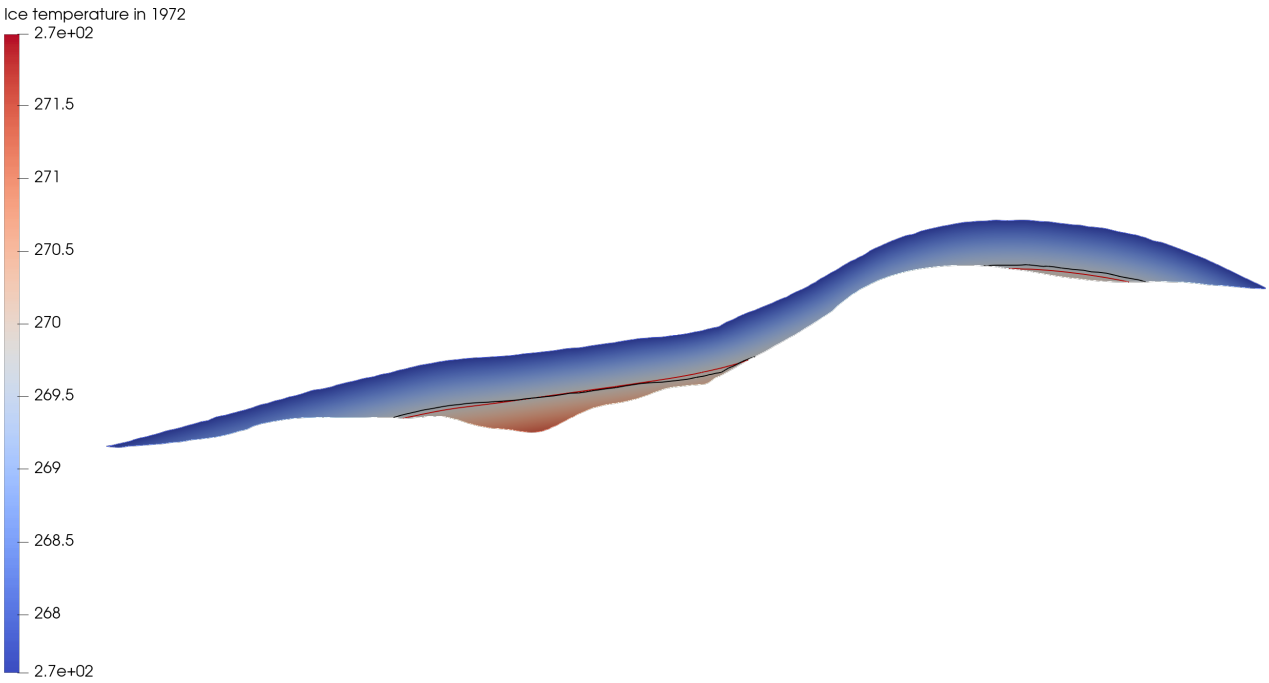

Figure 5.6: Temperature profile of the glacier ice taken approximately from Stake N, through to Stake FL3. The red isoline marks a temperature of -3.3 °C and the black isoline marks a depth of 65 meters. Temperature range of the figure is from 267.5K to 272K; colder ice is colored blue while warmer ice is colored red. This figure was used to verify correct model ice temperatures and the results are a close match with [Liestol, 1974].

An example of the glacier ice temperature is presented in Figure 5.6. The figure is a vertical slice taken across the entire glacier on a line situated along ablation stake N on the ice cap, through to stake FL3 on the valley glacier. This was simulated by assuming a constant atmospheric temperature of 267.6K and a constant basal heat flux of 67 mW m^2. The model takes into account frictional and deformational heating, but not warming due to other factors. The geometry of the model is that of the 1961 glacier which was assumed to be close enough match with 1972, although some thinning is likely to have occurred during the 11-year interlude.

Isochrone distribution

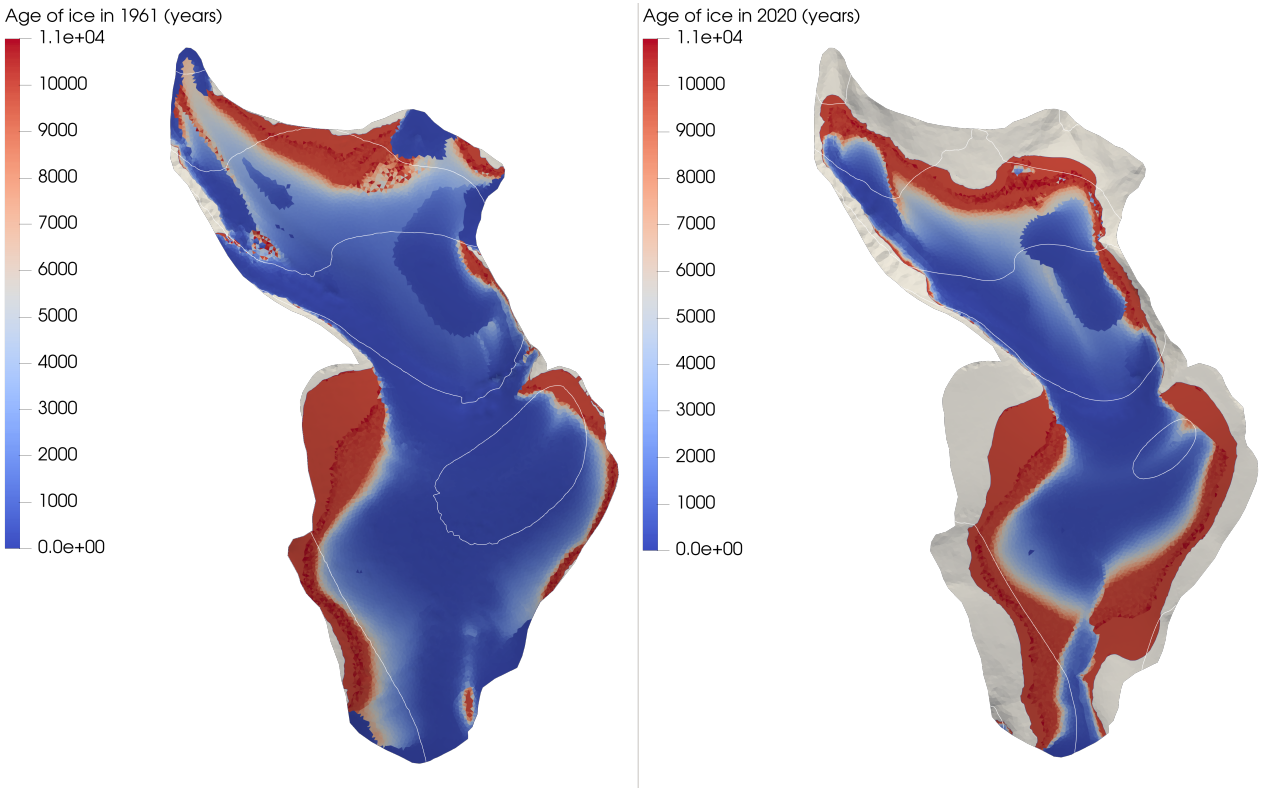

Figure 5.7: Isochrone distribution of the surface ice of the Foxfonna glacier system in 1961 (left) and 2020 (right). Upper Foxfonna age distribution ranges from new ice to ice that is around 5000-10000 years old near the margins and within the core glacier. Younger ice is colored blue, while older ice is colored red. The transition goes through a white color, which corresponds to around 5500 years of age. The white isoline represents the surface elevation in steps of 100 meters.

The isochrone distribution (i.e. age of the ice) of the Foxfonna glacier system in a steady state is presented in Figure 5.7 (surface distribution), and Figures 5.8, 5.9 (two vertical profiles of the ice cap). In general the age of the ice on the ice cap ranges up to 5000-10000 years, similar values are found at the margins and NE tongue of the valley glacier. This simulation, as others based upon the 2020 DEM has error and outliers near the very edges of the mountaintops. However these do not impact the simulation on the glacier itself, but merely affect the visualization of the results.

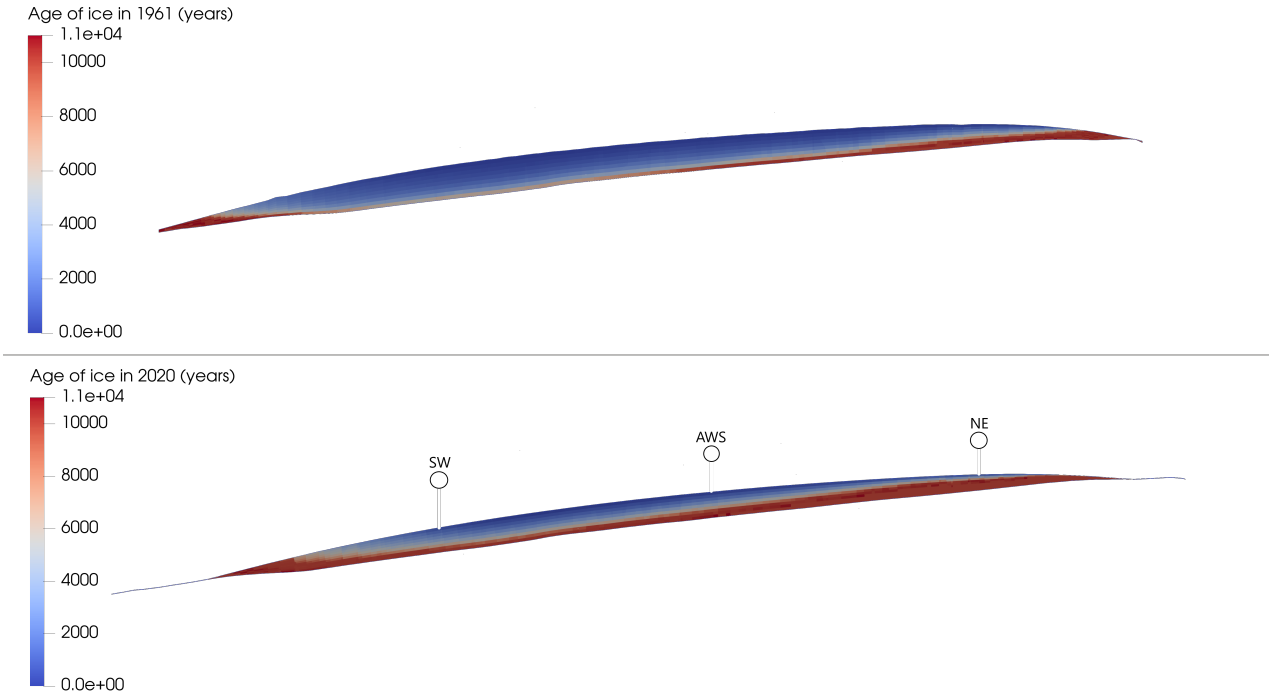

Figure 5.8: Two vertical isochrone profiles of the Foxfonna ice cap from 1961 and 2020. The profile is taken along the SW-AWS-NE line (see Figure 5.10). Younger ice is colored blue, while older ice is colored red.

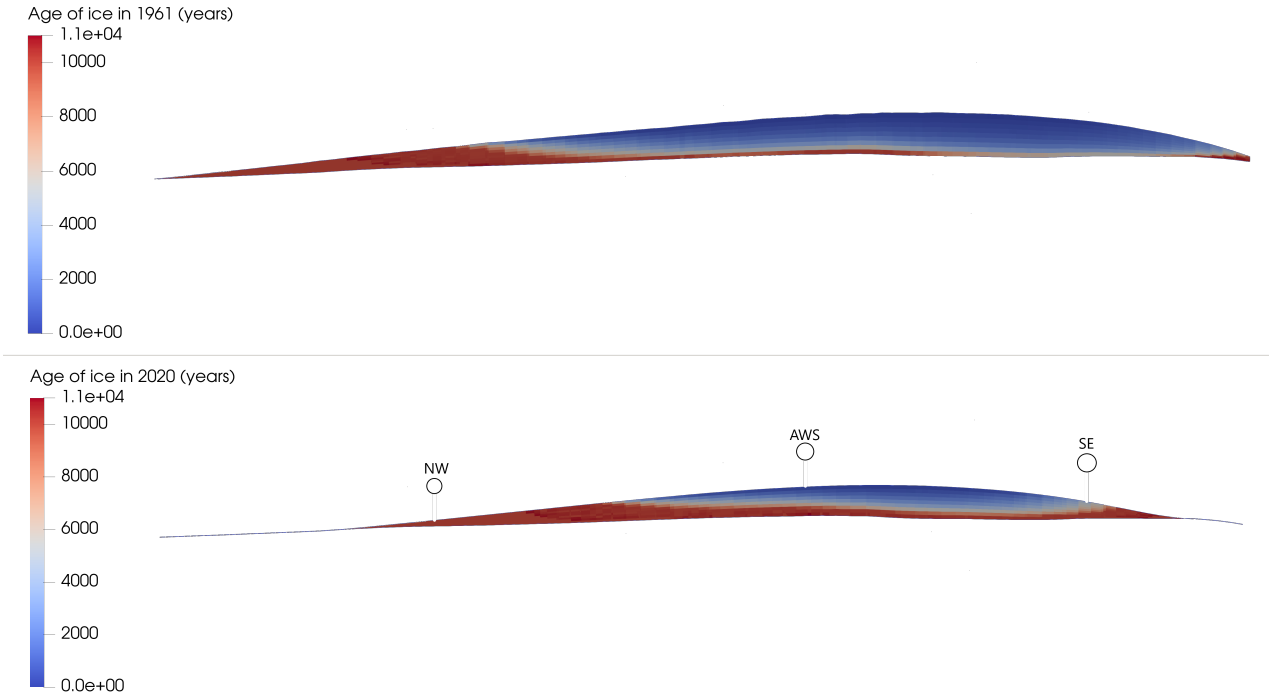

Figure 5.9: Two vertical isochrone profiles of the Foxfonna ice cap from 1961 and 2020. The profile is taken along the NW-AWS-SE line (see Figure 5.10). Younger ice is colored blue, while older ice is colored red.

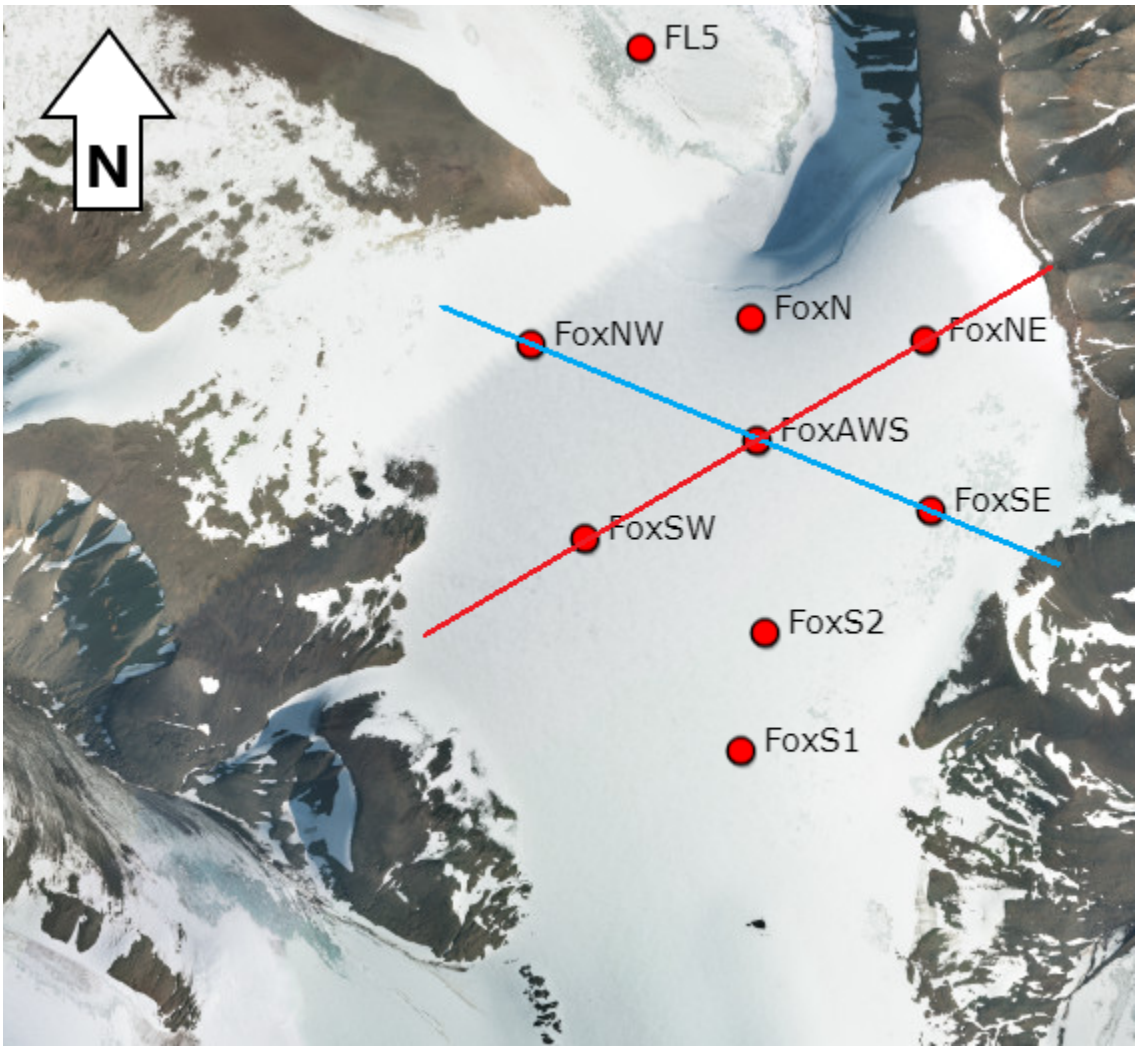

Figure 5.10: Representation of the two paths the vertical profiles were taken along, as seen in Figure 5.8 (red line) and Figure 5.9 (blue line). Image courtesy of the Norwegian Polar Institute (https://toposvalbard.npolar.no/).

Surface mass balance models

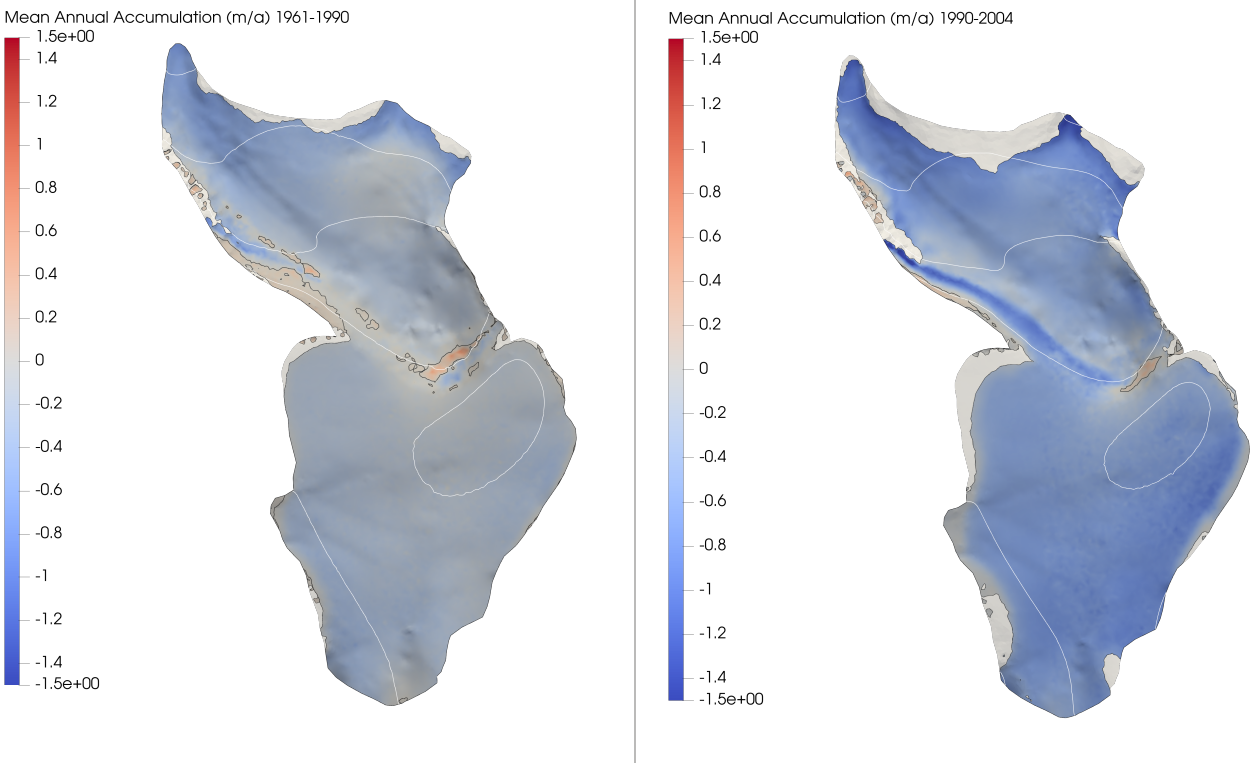

Figure 5.11: Mean surface mass balance of the Foxfonna glacier system for the interval of 1961-1990 (left) and 1990-2004 (right). Areas colored blue denote mass loss, while red areas represent areas which gained mass during the time period. The thin dark line marks the equilibrium-line. The white isoline represents the surface elevation in steps of 100 meters.

The surface mass balance of the entire glacier system was simulated between the years 1961 and 2020. This method has previously been used in [Välisuo et al., 2017] and is summarised in Section 4.4, "Surface mass balance". The arithmetic mean of the glaciers of 1961-1990, 1990-2004, 2004-2009, and 2009-2020 were used in the simulations. See Figure 5.11 for simulations from 1961 to 2004, and Figure 5.12 for simulations from 2004 to 2020. The scale of negative 1.5 m/a to positive 1.5 m/a was chosen to accurately portray the annual mean accumulation and provide better contrast to the actual glacier, as values exceeding those only occurred in the 1990-2004 simulation and were most likely a consequence of errors in the elevation model. The sharp positive accumulation on the mountainside in the 2009-2020 model is definitely an error in the field method used and discussed in Section 3.4.1, "Quality of the elevation models".

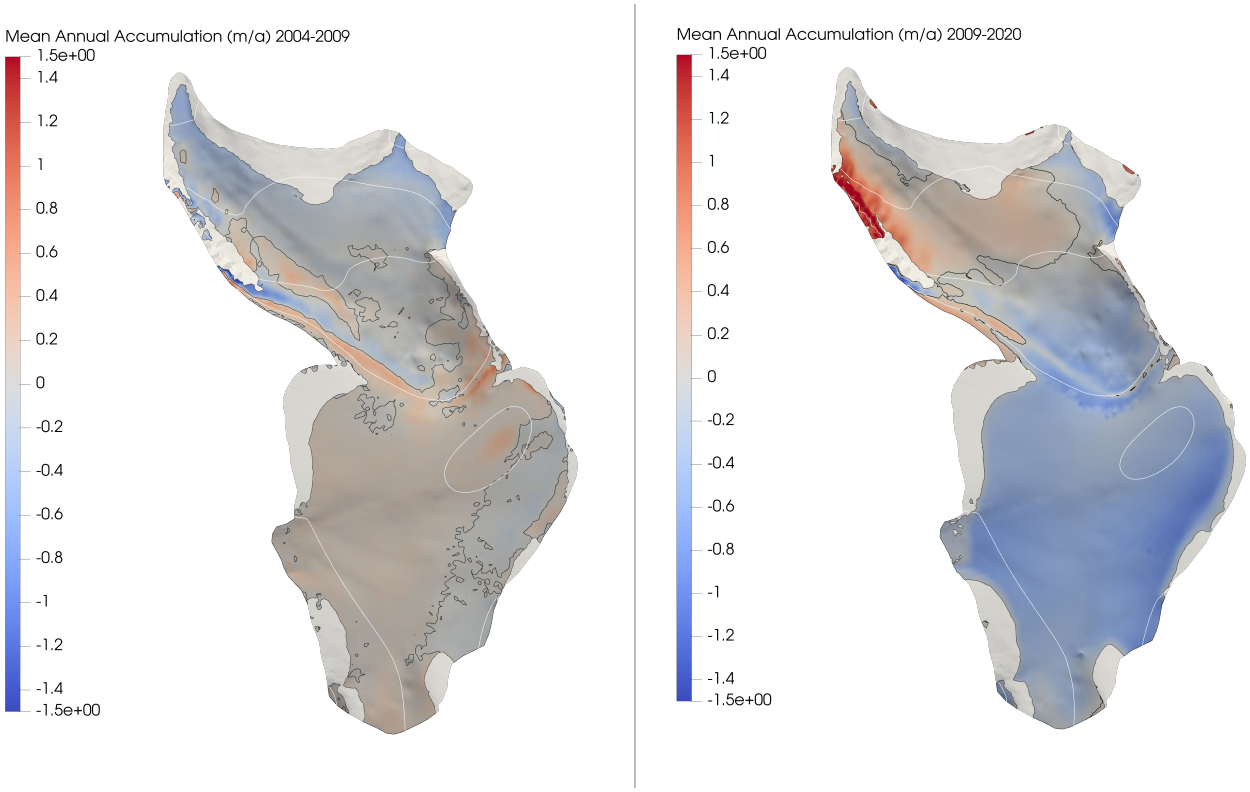

Figure 5.12: Mean surface mass balance of the Foxfonna glacier system for the interval of 2004-2009 (left) and 2009-2020 (right). Areas colored blue denote mass loss, while red areas represent areas which gained mass during the time period. The thin dark line marks the equilibrium-line. The white isoline represents the surface elevation in steps of 100 meters.

Location	Model 04-09 Bn (m)	Obs. 07-09 Bn (m)		Model 09-20 Bn (m)	Obs. 09-20 Bn (m)
NW	0.07	0.01		-0.45	-0.46
SW	0.1	0		-0.58	-0.52
AWS	0.1	0.04		-0.38	-0.40
N	0.22	0.09		-0.28	-0.32
NE	0.32	0.01		-0.42	-0.38
SE	-0.1	-0.37		-0.84	-0.80
S1	0	-0.07		-0.62	-0.61
S2	0.03	-0.21		-0.58	-0.57

Table 5.3: Comparison between the geodetic surface mass balance model and an averaged value for surface changes observed in situ between the years 2007-2009 and 2009-2020. Change in thickness given in meters (m). Note that a complete temporal overlap of the geodetic and glaciological observations only occurs 2009-2020.

6. Discussion & Conclusions

Discussion will be split into 3 short sections pertaining to each relevant focus area of the simulations: (1) verification of the results, (2) isochrone model, and (3) surface mass balance model. The verification of the model results entails the comparison of the simulated results to the observed ice temperature and flow velocities. Although the surface mass balance model could be verified in a similar manner this will be done in its own section.

6.1 Ice temperature

To ensure the simulations were as realistic as possible it was attempted to match the glacier surface ice velocity and ice temperature with in-situ observations. The glacier ice temperature was matched with measurements made in 1972, and an attempt was made to match glacier surface ice velocity with observations made between 2012-2014.

Ice temperature was matched with the values observed by [Liestol, 1974] (see Figure 5.6), but this required an unrealistically warm atmospheric temperature of 267.6K (-5.55°C). This value is slightly warmer than the 30-year climatic average of -6.0°C (1957-1987) at sea level. Accounting for elevation with the lapse rate the mean temperature should be roughly 3°C colder for the elevation the 1972 observations were taken at. This deviation from observed temperatures may be due to the model's inability to take into account heating due to firn or superimposed ice (See Section 2.1.2, "Thermodynamics of glaciers"), heat transport by englacial water channels, or a poor observation in the aforementioned publication.

The fitted value for the mean air temperature (-5.55°C) was used in all simulations, although the region saw almost 2°C of warming during the time period. While the observed atmospheric warming does improve the fit for the temperature parameter it is still an apparently too warm a value for the elevation. Furthermore between 1961 and 2020 the glacier has lost nearly all of its firn layer and throughout the entire glacier system the snow cover no longer survives over the melting season. The glacier is therefore no longer warmed up from the release of latent heat due to refreezing under the firn or snow cover which can be a significant source of energy, thus effectively cooling the ice. With these two effects: atmospheric warming and latent heat due to refreezing, working to counter each other, as well as uncertainty in the initial value it is difficult to be certain on what parameter to use in 2020. However as the temperature stays above -10°C in both cases it does not affect the creep relation, as the model uses constant values for creep parameters at this temperature range - a widely accepted and reasonable approximation [Cuffey and Paterson, 2010].

A large temperate ice area near the bed of the Foxfonna valley glacier was suggested by [Cheung, 2021], with a thickness of some 5 to 25 meters. While a temperate bed would not be impossible for Foxfonna it seems highly unlikely that nearly a quarter of the glacier thickness would be temperate, but this may occur due to meltwater seeping into the glacier bed vie e.g. crevasses [Cheung, 2021]. As a comparison, Midtre Lovénbreen - a relatively similar small valley glacier - is suspected to only have temperate ice at its thickest section which is in excess of 120 meters [Välisuo et al., 2017]. However the release of latent heat due to refreezing of water on the glacier surface was believed to have a more of an effect on warming the bed, rather than ice thickness.

6.2 Surface ice velocity

The Foxfonna glacier system is a slow moving mass of ice. Velocities only exceed 1 m/a on the steep slope connecting the ice cap to the valley glacier, and briefly on a single flow path towards the NE tongue. A clear change from 1961 to 2020 can be seen in the near total loss of ice flow (simulated) across the glacier. The glacier in 2020 was frozen to its substrate as is evident both in in situ measurements on the ice cap in 2012-2014 and simulated velocities.

The flow paths taken by the glacier are visible in the 1961 simulation (Figure 5.3, left-side). There are four main paths of flow: (1) from the top of the ice cap towards the NE outlet of the valley glacier, (2) from the top of the ice cap down towards the NW outlet of the valley glacier, (3) from the top of the ice cap down towards Rieperbreen, (4) radially outwards into the direction of SW-SE from the top of the ice cap. Little to no ice flow appears to occur towards the NE and NW from the ice cap. This is likely due to the flow being directed down into the valley glacier.

Ice flow was faster in 1961. Between 1961 and 2020 the glacier surface flow has slowed down between 0.3 to 1.5 m/a, thus altering the velocity distribution. By 2020 the surface flow of ice between Foxfonna ice cap and Rieperbreen (3) seems to have ceased and any radial flow (4) on the upper ice cap is limited to the SW flow path (Figure 5.3). The fastest simulated ice flow is at the slope connecting the ice cap to the valley glacier. A maximum ice velocity of 2.2 m/a is modelled in the central slope, however by 2020 these velocities have decreased by more than half, to around 0.8 m/a. Other regions of "fast" flowing ice includes the north-eastern tongue of the valley glacier - which has melted out by 2020 - and the southern tongue connecting to Rieperbreen.

The glacier surface velocities of the simulation using the 2020 elevation model was attempted to be fitted onto the 2012-2014 observations [Koziol, 2014]. The magnitude of the velocities on the ice cap is an exact match at a few stakes, and close match at most. However as the velocities

are under 0.2 m/a at all but one stake it is safe to say that the model and observations are in agreement that the glacier ice is immobile.

The exception to the rule is the stake SE. In situ measurements using differential GPS record the magnitude of the ice flow at nearly 1 m/a on a slope of 9° to 12° (2021). This is four times that of stake SW, which is situated at a comparable, albeit thicker section of the glacier. Furthermore the direction of the observed flow is perpendicular to the elevation gradient, which defies common sense. No solid explanation on this velocity anomaly exists either in [Koziol, 2014] or in the field notes the author provided, nor is the underlying topography at a considerable angle. Without repeat measurements at the site we can only speculate as to why, but the author did provide information that heavy melting was likely occurring at that point of the ice cap. A similar issue was the likely - although uncertain - culprit for the lack of in situ data on three out of six ablation stakes located on the valley glacier.

Velocities observed on the valley glacier in 2012-2014 are faster than the simulated values of a healthier glacier in 1961. The fastest velocities on lower Foxfonna were measured near the glacier tongue, at almost 3 m/a at thickness of ~40 meters. The model is unable to replicate this velocity behaviour, rather the velocity decreases slightly towards the tongue as one would expect to occur as the thickness of the glacier decreases. At stake FL3 the velocity is only a tenth of what it is further down the flow path. Both stakes FL2 and FL3 are slightly off the simulated flow path (stake locations; refer to Figure 3.1). This suggests that sections of ice perpendicular to the direction of the flow at FL3 may exceed the velocity measured. In general the flow velocities measured are similar to that of cold-based tongues of larger glaciers such as [Nuttal et al., 1997], ~1 m/a, but the tongues are more than twice as thick as that of Foxfonna.

The field measurements on the valley glacier velocities may have been affected by external factors, such as excessive melting. Directly comparing the simulated values to the single set of observations made in 2012-2014 is not optimal. Out of six ablation stakes placed on the valley glacier, only half produced in situ data on the velocity distribution. The three locations

which we have data for suggest very erratic flow behaviour for which there is no clear physical explanation for at the moment. The lack of data from stakes FL1, FL4, FL6 is uncertain, as details provided on the field notes by the author [Koziol, 2014] were inconclusive, but suggested that the ablation stakes may have melted out entirely; this would make it impossible to obtain a velocity measurement at these sites. Had the ablation stakes on the valley glacier been used for measuring surface mass balance in 2013-2014 it may have been possible to confirm afterwards if they still existed during the second set of observations by differential GPS.

Choice of parameters

The simulated solution to the velocity distribution of the domain heavily affects the isochrone distribution, and to a degree the surface mass balance simulations as well through emergence velocity. Flow velocities for the glacier extents of 1961 and 2020 were each simulated with an assumption of steady-state and with an enhancement factor occurring in Glen's flow law of E=1. A larger value for the enhancement factor was unreasonable to use for two primary reasons: (1) it did not prove a better fit to observations e.g. some model-observation comparisons worsened while others improved, (2) a larger Glen's enhancement factor proved an impractical way of matching the velocities on the lower glacier to observations, as it would require an unrealistically large Glen's enhancement factor (> 10). This consideration is compounded by the fact that there is only one set of velocity measurements for both glaciers and due to the lack of repeat measurements an error in the field method cannot be ruled out.

The addition of basal sliding to parts of the glacier was attempted in order to match velocities observed on the lower glacier. The attempt was unsuccessful due to the claimed temperate regions of the lower glacier not adhering clearly to any specific parameter such as ice thickness or temperature. Furthermore due to strong evidence suggesting the glacier system is cold-based in nature is a more reasonable option to use a non-enhanced value until more information on the glacier velocities can be garnered. The use of a non-enhanced value is supported by [Cuffey and Paterson, 2010], where a value of 1 to 2.5 is recommended for younger ice, and in publications such as [Zwinger et al., 2014], [Välisuo et al., 2017], where an E=1 is used for similar Svalbard glaciers.

6.3 Isochrone model

It is important to remain critical with age values given by these simulations as they assume a steady state, which for a rapidly melting glacier such as Foxfonna, is a poor assumption. Rather, the isochrone simulations provide information on where the oldest ice may lie, but poor detail on how old it is quantitatively. The implications of a steady state assumption and other issues in the method will be discussed at the end of this section.

The isochrone distribution on the Foxfonna resembles that of a common ice cap with ice accumulating at the top before heading downwards into the glacier core later emerging at the glacier margin (see Figure 5.7) in the south-west, west, and south-east. This is only disrupted by ice flow into the two outlet glaciers, Foxfonna towards the north and Rieperbreen towards the south, respectively, as well as in the north-east flank of the ice cap from where simulated ice does not flow at all towards the north-east. This may be due to a slightly tilted bed topography which inhibits NE flow at current ice thicknesses. The oldest ice simulated on the ice cap is around 9000-10000 years old and located around its radial margin (see Figures 5.8, 5.9).

The surface ice has not moved at all on the north-eastern flank of the ice cap since 1961, as seen in Figure 5.3. In situ observations of intact moss dated to around 1500 yr. provided by [Roche, 2021] (Table 3.4), as well as the general thickness of the ice being too thin for the dominant climate to have ever allowed basal sliding in this region of the ice strongly suggests that the NE section of the glacier ice has never flown by any substantial amount. However due to the assumption of a steady state this result is not entirely true, as in the past the ice may have flown in the NE; due to the melting taking place in the 20th century the true values for the age of the ice will deviate from the simulations. In particular the melting would expose older ice at the accumulation areas (blue) while ablation areas (white-red) would see the younger ice exposed as melting occurs. An elevation model of the glacier at a steady state, e.g. pre-1850's, is required in order to more accurately simulate whether this is absolutely true for the NE section.

Due to the very slow emergence velocity ($\pm$ 25 cm/a) upon the ice cap it seems unlikely that

post-industrial ice has survived upon the glacier surface. There are no consistent accumulation records available on Foxfonna or nearby glaciers between 1850-1950 and as such we can only speculate to the accumulation rates. Due to the small size and cold-based nature of the ice cap the accumulation rates have likely always been small. Over a time period of 170 years (time since 1850) the ice accumulated then would have travelled around 4.25 meters, if travelling at the emergence velocity of 2020. However even if the ice flowed 4 times faster for the entire time period, the ice would have flowed only 18 meters deep into the glacier. As most of the ice cap has melted by around 15-30 meters since 1961 it is unlikely for any post-industrial isochrone layer to have survived. A small possibility exists that there is a layer of such ice near stake N, which has seen the least melt (~12m) post-1961.

The age of ice trend for the ice cap and valley glacier remains similar, with older ice found at the margins of the ice cap (7000-9000 yr) and the tongues of the valley glacier (5000-8000 yr). The older (1961) simulation shows younger ages for the ice (1000-4000 yr) residing in the regions of the contemporary (2020) glacier. The results of the simulation using the 1961 DEM thus disprove the results seen in the simulation run on the contemporary geometry of Foxfonna. The age of the ice on the 2020 surface and margin of Foxfonna ice cap would be closer to 1000-2000 years old (i.e. the ice from 1961 which has melted out to), as the simulations produced from earlier DEMs provide more accurate velocities in terms of the historical glacier ice flow.

Comments on the method

Modelling the isochrones of a glacier with Elmer/Ice is useful if e.g. looking for layers of a specific age of ice for coring, but such models need to be verified and constrained by reliable in situ measurements of glacier surface velocity. These are nowadays possible to obtain by e.g. InSAR [Gourmelen et al., 2011], [Kumar et al., 2011]. But such data were not available for slow moving glaciers on Spitsbergen when searched for.

The steady state approach taken provides a poor estimate for the actual age of the ice on Foxfonna. The assumption of a glacier in steady state is often a necessity in order to keep the simulation simple, however in the current climate of glacier retreat it is no longer possible to completely rely on this approach for glaciers with a deeply negative mass balance, such as Foxfonna. The results given by the isochrone method are unsuitable for precise work, but rather provide a guideline on where the oldest ice may lie, but no good indication on the actual age.

6.4 Surface mass balance model

Modelling the surface mass balance of the Foxfonna ice cap provides an accurate visual method of seeing the general trends in surface mass balance along the entire glacier system. Provided with in situ measurements for comparison it is a way of filling in the gaps to visualize a long-term or near annual trend in surface mass balance, provided there are enough elevation models. While glacier flow is accounted for by including the effects of emergence velocity (see Section 4.4, "Surface mass balance") due to the very slow moving ice it has little effect; it affects the surface mass balance by at most 2.5 cm/a in both the positive or negative.

The surface mass balance models of Foxfonna suggest the glacier has had a consistently negative annual accumulation rate since 1961. This is best portrayed in Figure 5.11 which includes two long time-series on the simulated domain, from 1961 to 2004. These figures primarily showcase the long-term trend of the surface mass balance. However any single years of positive surface mass balance are not visible in these figures and there are no historical in situ observations available on the surface mass balance of individual years for this time period. While the simulation of 1961-1990 spans a total of 30 years the loss of surface ice was not as strong as in the shorter simulation of 1990-2004; when the annual loss of ice was nearly twice that of the earlier modelled period. The decreasing glacier extent makes it possible to see that it was during the period of 1990-2004 that the valley glacier began to rapidly lose mass at its tongues and on the slab of ice on the south-western mountainside.

Small-scale variations due to weather and topography are visible in the 2004-2009 model (Figure 5.12, left-side). This is the shortest time period between two consecutive elevation models, thus preventing the long-term mass loss trend from dominating the simulation. A comparison between the geodetic mass balance of 2004-2009 and the average mass balance of 2007-2009 can be found in Table 5.3.

The ice cap experienced positive mass balance on a large portion of its surface, primarily with an aspect from S to NE. The south-eastern side of the ice cap experienced a negative mass balance. Because in the wintertime the dominant wind direction from the south-east, it seems likely that we are able to see the effects of wind on accumulation patterns on the ice cap: a clean blown side at the SE while on the lee of the wind there is accumulation on the glacier surface and on the slope connecting the two halves of Foxfonna. A comparison between the model of 2004-2009 and in situ measurements of 2007-2009 is provided (see Table 5.3), however it was done mostly out of curiosity as the time periods are not an exact match. The comparison does show that the mean mass balance between 07-09 was more negative than the longer, modelled time period of 04-09. From the in situ measurements we are also able to see considerable loss of mass at stakes SE, S1, S2, i.e. the south-eastern side of the glacier. Thus it seems that the years with a considerably positive mass gain - as observed in the model of 2004-2009 - occurred earlier, between the years of 2004-2006.

The valley glacier primarily experienced mass loss over this time period with patches of positive mass gain near the mountainsides. This is possibly due to avalanche transport of snow to the glacier surface, as the trend is not repeated elsewhere on the glacier but the edges. Although the ice cap has experienced a mass gain on the lee side of the wind, the same did not seem to occur on most of the valley glacier. It is only possible to speculate. It may be that the mountainside to the SE shielded the valley glacier from wind transported snow deposition, or the entire cirque has acted as a wind tunnel allowing for any fresh precipitation to blow away soon after deposition.

The simulation of 2009-2020 (see Figure 5.12) matches the in situ surface mass balance measurements taken on the ice cap during the same time period. A comparison can be seen in Table 5.3. The ice cap as a whole is thinning, and the local spatial effects of weather on the free surface are still visible; the south-eastern to eastern flank has experienced more melt than the rest of the ice cap.

The accumulation dynamics of the lower glacier appear reversed for the model of 2009-2020 in comparison with the 2004-2009 model. At higher elevations the valley glacier is losing mass, while lower elevations are experiencing a modest, but positive mass balance. While the very positive areas of mass balance which are situated on the mountainsides may be due to systematic errors in the Structure from Motion method, it seems unlikely to be the case for a large area near the center of the surveyed domain. Also a product of the same elevation model produced near 1-to-1 match with the surface mass balance of the ice cap, suggesting the results for the lower glacier are reliable as well. It is unclear why this is the case and no in situ data of the mass balance on the valley glacier exists for the time period of this elevation model.

Comments on the method

Elmer/Ice provides a useful tool in producing 3D models of surface mass balance on a glacier. Digital elevation models in general provide an apparently accurate method for obtaining surface mass balance information on at least slow moving glaciers, and can be used to e.g. observe long-term or annual mass balance trends on the glacier surface. In slow moving glaciers the effect of the emergence velocity on the actual surface mass balance is small; a surface mass balance can be obtained without accurate information on the glacier velocities. This significantly lessens the workload, as you simply need to compare elevation models. In these cases a simpler geoinformatic systems program, e.g. ArcGIS [ESRI, 2021], QGIS [QGIS, 2021], can be used. However the faster the glacier flow is, the larger the error will be. Depending on the method used for the production of the elevation model different errors and deviations will exist. Any user needs to be aware of this, as well as assess the quality of the data they have at hand.

Bibliography

Adhikari, S. et al. (2012). *Modelling Dynamics of Valley Glaciers, Numerical Modelling.* InTech Europe, Rijeka, Croatia.

Andreassen, L. et al. (2016). Reanalysis of long-term series of glaciological and geodetic mass balance for 10 Norwegian glaciers. *The Cryosphere*, 10:535–552.

Benn D., E. D. (2010). *Glaciers and Glaciation, 2nd Edition.*

Betlem, P. (2018). Geothermal Gradients on Svalbard, Arctic Norway. *EAGE Joint Workshop on Deep Geothermal Energy, Strasbourg, France.*

Blaszczyk, M. et al. (2009). Tidewater glaciers of Svalbard: Recent changes and estimates of calving fluxes. *Pol. Polar Res.*, 30(2):85–142.

Brugger, K. (2007). The non-synchronous response of Rabots Glaciär and Storglaciären, northern Sweden, to recent climate change: a comparative study. *Annals of Glaciology*, 46:275–282.

Cai, B. et al. (1986). Mathematical models of the temperature and water-heat transfer in the percolation zone of a glacier. *Cold Regions Science and Technology*, 12:39–49.

Cheung, W. Y. (2021). Surface and bed topography mapping of Foxfonna and Rieperbreen glacier, Svalbard, 1936-2020. Master's thesis.

Christiansen, H. et al. (2005). Permafrost in the gruve-7 mine, adventdalen, svalbard. *Norsk Geografisk Tidsskrift - Norwegian Journal of Geography*, 59:2:109–115.

Compagno, L., Jouvet, G., Bauder, A., et al. (2019). Modeling the Re-appearance of a Crashed Airplane on Gauligletscher, Switzerland. *Front. Earth Sci.*, 7.

Cuffey, K. and Paterson, W. (2010). *The Physics of Glaciers*. Butterworth-Heinemann/Elsevier.

Divine, D. and Dick, C. (2006). Historical variability of sea ice edge position in the nordic seas. *Geophys. Res. Lett.*, 111.

Doherty, S. et al. (2010). Light-absorbing impurities in Arctic snow. *Atmos. Chem. Phys.*, 10:11647 – 11680.

Duval, P. et al. (1980). Crystal size and climatic record down to the last ice age from Antarctic ice. *Earth and Planetary Science Letters*, 48:59–64.

D'Andrea, W. et al. (2012). Mild little ice age and unprecedented recent warmth in an 1800 year lake sediment record from svalbard. *Geology*, 40(11):1007–1010.

Edwards, T. et al. (2021). Projected land ice contributions to twenty-first-century sea level rise. *Nature*, 593:74–82.

Edwards, T., Nowicki, S., et al. (2014). Effect of uncertainty in surface mass balance–elevation feedback on projections of the future sea level contribution of the Greenland ice sheet. *The Cryosphere*, 8:195–208.

ESRI (2021). Environmental Systems Research Institute (ESRI). http://www.esri.com. Accessed: 2021-12-13.

Flanner, M. et al. (2007). Present-day climate forcing and response from black carbon in snow. *Journal of Geophysical Research: Atmospheres*, 112(D11).

Fowler, A., Ng, F., et al. (2019). *Glaciers and Ice Sheets in the Climate System*.

Gagliardini, O., Fillet-Chaulet, F., Durand, G., Vincent, C., and Duval, P. (2011). Estimating the risk of glacier cavity collapse during artificial drainage: the case of Tête Rousse Glacier. *Geophys. Res. Lett.*, 38(L10505).

Gagliardini, O., Zwinger, T., Fillet-Chaulet, F., Durand, G., et al. (2013). Capabilities and performance of elmer/ice, a new generation ice-sheet model. *Geosci. Model Dev.*, 6:1299–1318.

Geuzaine, C. and Remacle, J.-F. (2009). Gmsh: a three-dimensional finite element mesh generator with built-in pre- and post-processing facilities. *International Journal for Numerical Methods in Engineering*, 79(11):1309–1331.

Gilbert, A. et al. (2018). Mechanisms leading to the 2016 giant twin glacier collapses, Aru Range, Tibet. *The Cryosphere*, 12:2883–2900.

Gourmelen, N. et al. (2011). Ice velocity determined using conventional and multiple-aperture InSAR. *Earth and Planetary Science Letters*, 307(1-2):156–160.

Greve, R. and Blatter, H. (2009). *Dynamics of Ice Sheets and Glaciers*.

Haeberli, W. et al. (1991). Borehole temperatures at the Colle Gnifetti core-drilling site (Monte Rosa, Swiss Alps). *Journal of Glaciology*, 37(125):37–46.

Hagen, J.-O. et al. (1993). *Glacier Atlas of Svalbard and Jan Mayen*.

Hanssen-Bauer, I. et al. (2019). Climate in svalbard 2100 – a knowledge base for climate adaptation. *Norway, Norwegian Centre of Climate Services (NCCS) for Norwegian Environment Agency (Miljødirektoratet), (NCCS report 1/2019)*.

Hodson, A. et al. (2007-2020). Annual mass balance measurements on Foxfonna glacier - some data published.

Holmlund, E. S. (2020). Rapid temperature rise may have triggered glacier surges all over Svalbard. Master's thesis.

Isaksen, K. et al. (2000). Ground surface-temperature reconstruction based on data from a deep borehole in permafrost at Janssonhaugen, Svalbard. *Annals of Glaciology*, 31(1):287–294.

Isakson, E. et al. (2005). Climate oscillations as recorded in Svalbard ice core O18 records between AD 1200 and 1997. *Geografiska Annaler: Series A, Physical Geography*, 87(1):203–214.

Jouvet, G. et al. (2020). Mapping the age of ice of Gauligletscher combining surface radionuclide contamination and ice flow modeling. *The Cryosphere*, 14:4233–4251.

Karypis, G. and Kumar, V. (1999). A Fast and Highly Quality Multilevel Scheme for Partitioning Irregular Graphs. *SIAM Journal on Scientific Computing*, 20(1):359–392.

Koerner, R. et al. (1979). Discontinuous flow, ice texture, and dirt content in the basal layers of the devon island ice cap. *Journal of Glaciology*, 23(89):209–222.

Kohler, J. et al. (2003). Temperature and precipitation, late 19th century to the present. *ACIA Final Report: 21.*

Kohler, J. et al. (2007). Acceleration in thinning rate on western svalbard glaciers. *Geophysical Research Letters*, 34(L18502).

Koziol, K. (2014). *The Provenance, Composition, and Fate of Organic Carbon on an Arctic Glacier (PhD thesis).* PhD thesis.

Kumar, A. et al. (2010). Contribution of sea ice loss to Arctic amplification. *Geophysical Research Letters*, 37(21).

Kumar, V. et al. (2011). Glacier surface velocity estimation using SAR interferometry technique applying ascending and descending passes in Himalayas. *International Journal of Applied Earth Observation and Geoinformation*, 13(4):545–551.

Legrand, M. et al. (1988). Vostok (Antarctica) ice core: Atmospheric chemistry changes over the last climatic cycle (160,000 years). *Atmospheric Environment*, 22(2):317–331.

Liestol, O. (1974). Glaciological work in 1972. *In Årbok 1972, Norsk Polarinstitutt: Oslo*, pages 125–135.

Liestol, O. (1993). Glaciers of Europe - Glaciers of Svalbard, Norway. *U.S. Geological Survey Professional Paper*, 1386-E-5.

Malles, J.-H. et al. (2021). Twentieth century global glacier mass change: an ensemble-based model reconstruction. *The Cryosphere*, 15(7):3135–3157.

McNabb, R. (2018). Sensitivity of glacier volume change estimation to dem void interpolation.

Mokhov, I. et al. (2006). Tropospheric lapse rate and its relation to surface temperature from reanalysis data. *Izv. Atmos. Ocean. Phys*, 42:430–438.

NKSS (2021). Norsk klimaservicesenter: Seklima - observasjoner og værstatistik. https://seklima.met.no/. Accessed: 2021-07-13.

Nordli, O. et al. (2014). Long-term temperature trends and variability on spitsbergen: the extended svalbard airport temperature series, 1898-2012. *Polar Research*, 33.

Nuth, C. et al. (2013). Decadal changes from a multi-temporal glacier inventory of Svalbard. *The Cryosphere*, 7:1603–1621.

Nuttal, A.-M. et al. (1997). Quiescent-phase changes in velocity and geometry of Finsterwalderbreen, a surge-type glacier in Svalbard. *Annals of Glaciology*, 24:249–254.

O'Neel, S. et al. (2019). Reanalysis of the US Geological Survey Benchmark Glaciers: Long-term insight into climate forcing of glacier mass balance. *Journal of Glaciology*, 65(253):850–866.

Painter, T. et al. (2013). End of the Little Ice Age in the Alps forced by industrial black carbon. *Proceedings of the National Academy of Sciences*, 110(38):15216 – 15221.

Peyaud, V. et al. (2020). Numerical modeling of the dynamics of the Mer de Glace glacier, French Alps: comparison with past observations and forecasting of near-future evolution. *The Cryosphere*, 14:3979–3994.

Pfeffer, W. A. et al. (2014). The Randolph Glacier Inventory: A globally complete inventory of glaciers. *Journal of Glaciology*, 60(221):537–552.

QGIS (2021). QGIS Geographic Information System. QGIS Association. http://www.qgis.org/. Accessed: 2021-12-13.

Rabus, B. and Echelmeyer, K. (2002). Increase of 10 m ice temperature: Climate warming or glacier thinning? *Journal of Glaciology*, 48(161):279–286.

Roche, A. (2021). Neoglacial plateau ice cap behaviour in central spitsbergen constrained by subglacially preserved vegetation. Master's thesis.

Rutter, N. et al. (2011). Hydrology and hydrochemistry of a deglaciating high-Arctic catchment Svalbard. *Journal of Hydrology*, 410(1-2).

Råback, P., Malinen, M., Ruokolainen, J., Pursula, A., and Zwinger, T. (2022). Elmer Models Manual https://www.nic.funet.fi/index/elmer/doc/ElmerModelsManual.pdf. Accessed: 2022-02-08.

Salinger, J. et al. (2008). Glacier response to climate change. *Water and Atmosphere*, 16(3):16–17.

Schwikowski, M. and Eichler, A. (2010). *Alpine Glaciers as Archives of Atmospheric Deposition, The Handbook of Environmental Chemistry*, volume 6. Springer, Berlin, Heidelberg.

Seddik, H., Greve, R., and Zwinger, T. (2012). Simulations of the Greenland ice sheet 100 years into the future with the full Stokes model Elmer/Ice. *Journal of Glaciology*, 58(209):427–440.

Stone, P. et al. (1979). Atmospheric Lapse Rate Regimes and Their Parameterization. *Journal of the Atmospheric Sciences*, 36(3):415–423.

Vaughan, D. et al. (2013). Observations: Cryosphere. In: Climate Change 2013: The Physical Science Basis. Contribution of Working Group I to the Fifth Assessment Report of the Intergovernmental Panel on Climate Change. *Cambridge University Press*.

Välisuo, I., Zwinger, T., and Kohler, J. (2017). Inverse solution of surface mass balance of Midtre Lovenbreen, Svalbard. *Journal of Glaciology*, 63(240):593–602.

Zwally, H. et al. (2002). Surface Melt-Induce Acceleration of Greenland Ice-Sheet Flow. *Science*, 297(5579):218–222.

Zwinger, T., Moore, J., and Test, T. (2009). Diagnostic and prognostic simulations with a full Stokes model accounting for superimposed ice of Midtre Lovénbreen, Svalbard. *The Cryosphere*, 3:217–229.

Zwinger, T., Schäfer, M., et al. (2014). Influence of anisotropy on velocity and age distribution at Scharffenbergbotnen blue ice area. *The Cryosphere*, 8:607–621.